Journal of South American Earth Sciences 139 (2024) 104882



Contents lists available at ScienceDirect

Journal of South American Earth Sciences

journal homepage: www.elsevier.com/locate/jsames



Volcano tectonic setting of the Salares Norte Au–Ag epithermal belt, central Andes of northern Chile

J. Clavero [a,*], P. Pérez-Flores [b], F. Rojas [c], D. Huete-Verdugo [c], B. Droguett [a], V. Ramírez [a]

[a] Amawta Geoconsultores Ltda., Almirante Pastene 185 of. 503, Santiago, Chile
[b] Cigea Consultores Ltda., Manuel Rojas 23, Huasco, Chile
[c] Gold Fields Salares Norte SpA, Presidente Riesco 5561, 7th floor, Santiago, Chile

ARTICLE INFO

Keywords:
Salares Norte belt
Epithermal
Andes
Phreatomagmatic
Maar
HS

ABSTRACT

The Salares Norte (SN) Au–Ag belt is here defined as an Upper Miocene-Pliocene metallogenic area, extending for nearly 200 km, located NE of the northern end of the Upper Oligocene-Lower Miocene Maricunga Belt in the central Andes of northern Chile. The belt is located just east of the main reverse NS fault systems which are part of the Sierra Castillo, Potrerillos Mine and Claudio Gay Cordillera faults, limited to the north and south by the NW-striking oblique to the arc Imilac and Wheelwright-Incahuasi regional faults systems.

The epithermal deposits within the SN belt are intimately associated with the occurrence of Middle Miocene volcaniclastic basins and Middle to Upper Miocene phreatomagmatic vents and their related high-sulfidation hydrothermal systems. The volcanostratigraphy of the SN epithermal belt comprises volcaniclastic sequences, subvolcanic and volcanic rocks ranging between the Lower Miocene and the Pliocene. High-angle NS reverse faults involving Paleozoic and lower Cenozoic units form the western-southwestern limit of the belt. Folded and faulted Middle Miocene volcaniclastic and volcanic sequences form the main host rock of at least 4 phreatomagmatic events that generated maar-diatreme fields and discrete maar vents, with their related subvolcanic facies, within the widespread Upper Cenozoic volcanic arc, ranging in age between *ca.* 15 and *ca.* 4 Ma. These four phreatomagmatic events are spatially and temporarily associated to 4 main high-sulfidation hydrothermal events which have altered both the phreatomagmatic rocks and the Cenozoic country rock of the explosive activity. These hydrothermal systems have formed dozens of discrete hydrothermally altered areas where argillic, advance argillic, silicification and steam-heated alteration are common. Most of the maar fields and the hydrothermal alteration systems are emplaced within a strike-slip tectonic regime with NE-trending shortening which is accommodated in the NW-striking sinistral-normal faults and NE-striking extension structures. These fault systems crosscutting interaction favor the hydrothermal fluid circulation and migration, as well as mineral precipitation on structural and/or primary lithological traps and on NE-striking tension cracks.

In summary, the SN epithermal belt is an almost 200 km long and 60 km wide area, mainly NNE-oriented, where epithermal deposits have formed during the Upper Miocene and Pliocene (*ca.* 13-4 Ma), emplaced within Middle to Upper Miocene volcanic and volcaniclastic sequences associated to small volcanotectonic basins oriented in NS, NE-SW and NW-SE directions, in which most of the high-sulfidation systems are associated to discrete or repetitive structurally-controlled Upper Miocene-Pliocene phreatomagmatic vents and maar fields.

1. Introduction

The Andes of northern Chile present several Cenozoic epithermal belts which have been extensively explored and exploited in the last decades (Fig. 1) such as the Paleocene El Peñón-Guanaco belt (Warren et al., 2008; Jovic et al., 2015; Galina, 2019), the Oligocene-Miocene Maricunga belt (*e.g.* Sillitoe et al., 1991; Muntean and Einaudi, 2001; Gamonal et al., 2015) and the Upper Miocene El Indio belt (e.g. Araneda, 1982; Davidson and Mpodozis, 1991; Martin et al., 1995; Bissig et al., 2001).

The exploration of epithermal gold deposits East of the well-known Maricunga belt started only a couple of decades ago, later than in other areas with similar characteristics, probably due to the young age of the volcanic cover in this part of the Altiplano-Puna (e.g. Clavero et al.,

* Corresponding author.
E-mail address: jclavero@amawta.cl (J. Clavero).

https://doi.org/10.1016/j.jsames.2024.104882
Received 1 September 2023; Received in revised form 22 March 2024; Accepted 22 March 2024
Available online 28 March 2024
0895-9811/© 2024 The Authors. Published by Elsevier Ltd. This is an open access article under the CC BY-NC-ND license (http://creativecommons.org/licenses/by-nc-nd/4.0/).

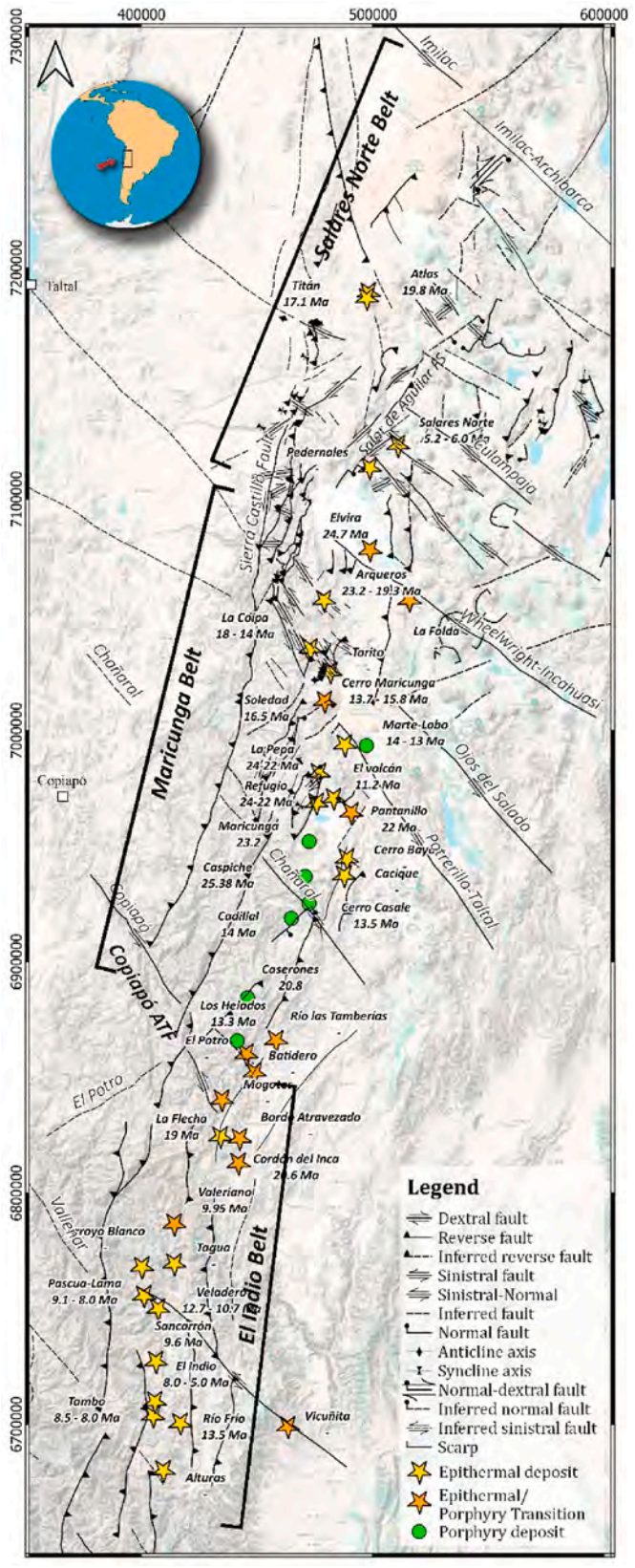


Fig. 1. Salares Norte Belt location.
Location and extension of the Miocene-Pliocene Salares Norte Au–Ag Belt, Central Andes and its relationship with the well-known Oligocene-Miocene Au–Ag Maricunga belt, and the Upper Miocene El Indio Belt.

1998, 2012; Gardeweg et al., 1998; Gardeweg et al., 1997 Naranjo et al., 2013a,b, 2016). More systematic exploration in this area started in the early 2000's, becoming more intense since 2011, after the discovery of economic gold mineralization in the Salares Norte district (Azevedo et al., 2015).

Here we present new stratigraphic, volcanic, tectonic and geochronologic data that indicates that the epithermal areas located ENE of the Maricunga belt at both sides of the Chile-Argentina border (Fig. 1) belong to a younger Au–Ag belt with its own structural and volcano-magmatic characteristics. Although there are strong evidences that the epithermal areas of this age and similar geotectonic and volcanic environment are also located on the Argentinian side, this study focuses on the Chilean part of the belt.

2. Methodology

This study is based on field mapping campaigns at different scales ranging from 1:50,000 to 1:10,000. Volcanological facies mapping was carried out mainly at 1:20,000 to 1,10.000 scale for volcanological reconstruction and projection of phreatomagmatic paleocraters. U–Pb radiometric data reported in this study were conducted at the Laboratory Zirchron LLC (Arizona, USA) at Washington State University (USA) using the LA-ICP-MS method. Thirty zircon grains were analyzed for samples corresponding to intrusive and effusive volcanic rocks, and between 50 and 70 grains for pyroclastic rocks. The ages obtained with the U–Pb method were calculated using Isoplot (Ludwig, 2003). Parameters and operating procedures like those suggested by Chang et al. (2006) were employed. Errors in U–Pb ages of zircon crystallization were obtained by quadratic summing of analytical errors plus the total systematic error in the analysis set (Valencia et al., 2005). The structural geology was mainly carried out in the field work, the collected structural data include description, measurement and logging of the geometry, kinematics, texture, mineralogy and crosscutting relationship of different structural elements (*i.e.* veins, fault-veins, hydrothermal breccias). Structural data collected was analyzed from regional scale. The stress field inversion was calculated by the Multiple Inversion Method (MIM). The MIM is based on a geometrical criterion (Yamaji, 2000), being a modification of the classic inverse technique of Angelier (1984). The method can calculate and sorting the orientation of the principal stress axes derived from a heterogeneous fault-slip data set by generating a combinatorial number of groups containing each k-number of fault-slip data elements extracted from the whole data set (Otsubo et al., 2006). Then it applies Angelier's (1984) inverse technique to all these randomly generated subsets. Finally, the orientations of the calculated stress axes for each generated group of k-number fault-slip data are plotted onto separate stereograms: one for σ1 axes and another for σ3 axes sub-solutions (Otsubo et al., 2006; Yamaji, 2000; Yamaji et al., 2006).

3. Tectonic setting

The South American tectonic setting is controlled mainly by the subduction plates, the Pacific under the South America. The style of the deformation is dominated by the orientation of the subduction vector, its obliquity with the trench, the velocity, the thermal conditions, and the mechanical condition in the inter-plate zone (e.g. Beck, 1991; Blanquat et al., 1998; Fossen et al., 1994; Hoffmann-Rothe et al., 2006; Mccaffrey, 1992; Teyssier et al., 1995). The convergence vector in the Central Andean segment at the northern Chile, records several changes in the obliquity, and velocity. The main changes describe are date at 26 Ma, 20 Ma, 16 Ma, 11 Ma, and 5 Ma. (Hoffmann-Rothe et al., 2006; Somoza, 1998). These variations are temporally associated with the tectonic regimes recorded in the parallel to the trench, Precordilleran Fault System (23°–27°). This fault system records a right-lateral strike slip kinematics since the ~30 Ma, which changes to left-lateral strike slip between 16 and 6 Ma, to become oblique dextral-reverse up to the present

(Hoffmann-Rothe et al., 2006).

In the regional context, the Andean Mountain range hosts numerous mineral deposits including giant copper porphyries (e.g. Chuquicamata, Rio Blanco-Los Bronces, El Teniente) and some of the world's largest epithermal deposits (e.g. Yanacocha, Veladero, El Indio) (Holley et al., 2016; e.g. Perelló et al., 2012; Piquer et al., 2015). In northern Chile, the El Indio and Maricunga belts, two of the main Cenozoic metallogenic domains, are arranged in NS-orientation, located between 26° and 30° (e.g. Mpodozis and Kay, 2003, Fig. 1). The different Au–Ag–Cu ore deposits are distributed in a complex permeability architecture mainly formed by the interaction between reverse NS-striking arc-parallel faults, and NW- and NE-striking Arc-Transverse Faults (ATF) (e.g. Giambiagi et al., 2017; Holley et al., 2016; Niemeyer and Munizaga, 2008; Palacios et al., 2007; Piquer et al., 2019; Yáñez and Rivera, 2019).

The distribution of different styles of ore deposits is marked by a predominance of porphyry Au–Cu deposits in the segment defined between the NW-striking Arc Transverse Faults (ATF), Copiapó, and Potrerillos-Taltal. The Potrerillos-Taltal ATF marks a boundary from which the distribution of ore deposits is wider to the north than southern segment (Fig. 1), while the Copiapó ATF is the limit between the El Indio and Maricunga belts. This ATF is located in a tectonic transition (26° S), where the normal becomes a horizontal subduction zone. The southern end of the normal subduction zone records the last active volcanic centers in the Pleistocene-Holocene at 27° S (e.g. Stern et al., 2007), including the volcanoes and volcanic complexes Nevado Ojos del Salado, Nevado Tres Cruces, Incahuasi, San Francisco, and Fraile (e.g. Mpodozis et al., 1996; Gardeweg et al., 1997, 1998; Clavero et al., 2012; Grosse et al., 2018). This flat-slab segment extends from 28° to 33° 30′S (e.g. Kay et al., 1999; Martinod et al., 2010), and records the onset of its horizontalization at ~12 Ma (e.g. Hu et al., 2016), although its present-day geometry, without asthenospheric wedge would have finished forming at 6–7 Ma (e.g. Kay et al., 2006), which coincides with the end of the volcanic activity in this segment, although small, sparse remnants of Pliocene domes have been reported in the El Indio Belt (Bissig et al., 2015).

The ages of the ore deposits range from 26 to 6 Ma (Oligocene to Upper Miocene) in the Main Cordillera, while older (Paleocene) ore deposits such as Guanaco and El Hueso of 48 and 40 Ma, respectively, are found on the western edge (e.g. Gamonal et al., 2015).

4. Salares Norte Au-Ag epithermal belt

4.1. Structural setting

The Salares Norte Au–Ag epithermal belt is here defined as a more than 200 km-long NNE-oriented and 60–80 km wide area, ENE of the well-known Maricunga belt, where abundant Middle Miocene to Pliocene epithermally altered areas occur within mainly Upper Cenozoic volcanic rocks. The belt is limited to the north and south by NW-striking regional deep and long lived fault systems: Imilac-Archibarca lineament (Richards and Villeneuve, 2002; Richards et al., 2013; Yáñez and Rivera, 2019) to the North and Incahuasi-Wheelwright lineament (Clavero et al., 2012) to the South (Fig. 1).The NW-striking Arc Transverse Faults has been recognized by geophysics anomaly, volcanic centers alignments and geomorphologic evidences (Viramonte and Petrinovic, 1985; Chernicoff et al., 2002; Richards and Villeneuve, 2002; Yáñez and Rivera, 2019). These NW-striking fault systems control the geometry of several volcanic centers and deposits, like Carachipampa-Farellón Negro, Corrida de Cori, and Chato Aislado Caldera (Richards and Villeneuve, 2002; Seggiaro et al., 2007). These NW-striking fault systems cut the NS-striking reverse fault systems, which in the southern area exhume part of the Paleozoic basement and deform the Oligo-Miocene volcano-sedimentary sequence in the Claudio Gay and Sierra Aliste Cordilleran (Mpodozis and Clavero, 2002; Clavero et al., 2012). The NE-striking fault systems in regional scale cut the NW-striking faults in the central area with the Salar de Aguilar Fault System (Fig. 1), whereas in the local scale this NE-striking structures are developed between NW-striking major faults like a secondary transfer faults and extensional fractures.

In the Salares Norte belt the main structural architecture is dominated by NS-, NW-, and NE-striking fault systems. The NS-striking faults have the least surface exposure, which are recognized by volcanic center alignment, and their geomorphological features that almost disappear in the northern area. The NW-striking fault systems record a sinistral and sinistral-normal kinematic with late normal displacement. These NW-striking fault systems are kinematically consistent along the belt, in the north the Laguna Azufrera Fault System (Fig. 2a), records wide fault zone with well exposed sinistral slickenside and fault planes (Fig. 2b and c). In the central area the Salares Norte Fault System consists of several NW-striking subparallel fault that define a NW-trending basin that host recent volcanic activity. Here, the NW-striking faults show the foliated fault core filled with jarosite and goethite up to 5 m wide (Fig. 2d), and late normal displacement (Fig. 2e). The NE-fault systems record manly dextral displacement and late normal kinematics. These structures are mostly developed between major NW-striking faults, but some of them crosscut. This fault system presents a wide fractured transtensional zones strongly altered (Fig. 2f) in the Horizonte area. In the Salares Norte the NE-striking fault records a multiples fault core with a wide damage zone pervasive altered (Fig. 2g) with kaolinite, jarosite, goethite, and quartz veins. In the northern area the NE-striking faults have similar characteristics, hosting strong altered zones with alunite-silica, and geomorphological scarp (~1 m) that cut Oligo-Miocene rock from the Laguna Azufrera sequence. Is common to find hydrothermal altered zones with characteristics of paleofumarolas NE-trending elongate, as well as phreatomagmatic and volcanic minor centers. The third order ENE-to WNW-striking sinistral transtensional structures are recognized mainly in the Salares Norte area (Fig. 2h and i).

For better geological understanding the Salares Norte Belt is divided into three segments, separated by NW-striking fault domains (Fig. 4). The Northern Laguna Azufrera-Aguas Caliente segment to the north of Laguna Azufrera Fault System, The Central segment Salar de Gorbea-Plato de Sopa, to the north of the Culampaja Fault System, and the Southern segment Salares Norte District, to the north of Incahuasi-Wheelwright Fault System.

4.1.1. Stress field analysis

The fault-slip inversion allows to calculate two regional stress fields (Fig. 3). The more represented is a transtensional stress field, with NNW-trending σ1, and ENE-trending σ3. The second solution is an extensional regime with NNW-trending σ1, and ENE-trending σ3. The first tectonic regime is compatible with sinistral NW-striking faults, and dextral NE-striking faults. The second tectonic regime is recorded mainly in intersection of these both fault systems, and in a late reactivation recorded in Salares Norte and Laguna Azufrera fault systems.

4.2. Geological setting

Fig. 4 shows a compilation map of the geology and main structures of the Salares Norte belt area. Data includes compilation from Clavero et al. (1998, 2012), Cornejo et al. (1998, 2009), Naranjo et al. (2013a, 2013b, 2016, 2019), Rubiolo and Pereyra, 2003, Seggiaro et al. (2006, 2007), Tomlinson et al. (1999), Villa et al. (2019) andZappettini et al., 2001, and this study.

The oldest stratigraphic units that crop out in the area are mainly located to the West and correspond to strongly folded and faulted Paleozoic and Mesozoic volcanic and sedimentary sequences, that form part of the basement of the Oligocene-Miocene Maricunga epithermal belt (Mpodozis et al., 1995; Mpodozis and Clavero, 2002). These units are strongly deformed and affected by folds and mainly reverse faults associated to several compressive deformation stages, the last of which occurred in the Lower Miocene. Scarce erosion windows occur on the



Fig. 2. Field structural mapping
(a) Photography looking to the NW, shows the core and damage zone of the Lagunilla Fault System, the fault planes record the sinistral slickenside (b) and (c). (d) NW-striking fault zone at the Brecha Principal segment from the Salares Norte Fault System. (e) Later normal displacement recorded in the NW-striking faults. (f) NE-striking transtension zone, strongly altered in the Horizonte area. (g) NE-striking transtensional zone with multiple fault core, wide damage zone with multiple veins. (h) WNW-striking sinistral fault zone strongly altered, and (i) horizontal slickenside.

Chile-Argentina border, giving rise to small-volume outcrops of mainly Permian granitoids. Unconformably overlying these units, on the western part of the area, were deposited a series of volcanic and volcanoclastic sequences of Eocene to Lower Miocene age (Tomlinson et al., 1999; Mpodozis and Clavero, 2002; Clavero et al., 2012), which are also folded and faulted by the Early Miocene compressive deformation with essentially NS axes, forming the western edge of the belt, where the Claudio Gay Cordillera and the Aliste Range are located. The younger of these, the Sierra de Aliste sequence (Clavero et al., 1998) is the equivalent of the local volcanic Infieles Sequence that forms the oldest basement unit on the western part of the belt. At the northern part of the belt, synchronically, the Lower Miocene Laguna de la Azufrera volcanoclastic sequence along with other less extended volcanoclastic sequences of the same age, previously unreported, developed associated to small

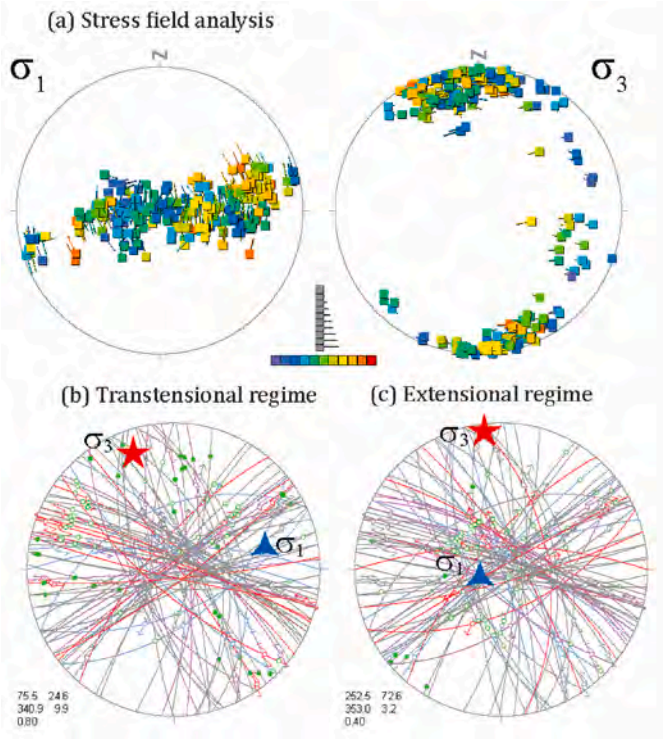


Fig. 3. Stress field solutions
(a) Stereographic projections show the principal stress axes analysis by Multiple Inverse Method (MIM) (Yamaji, 2000). (b) Transtensional regime solution and (c) extensional regime solution.

intermountain tectonically controlled basins. In the Lower Miocene a series of regional explosive events formed several ignimbrites that cover important parts of the area, especially to the central and northern areas of the belt. Some of these ignimbrites have been associated to large collapse calderas, one of which is inferred to cross the Salares Norte District area (Naranjo et al., 2019b), however no evidence has been found so far of such structure in the district. Unconformably overlying these units and associated both to the erosion of the topographic highs uplifted by the E-W compression and to the Middle Miocene volcanic/sedimentary sequences (16-12 Ma) a series of small-volume NS and NW-SE oriented basins formed, filled by volcanic and volcanoclastic material. These sequences, in the Salares Norte District (this study) are locally named as Salares Norte (ca. 16-13 Ma), Aster 2 (ca. 15-14 Ma) and Horizonte (ca. 14-12 Ma) sequences, in the northern part of the belt several outcrops of unnamed similar volcanoclastic sequences, previously unreported, also occur. Synchronically a series of stratovolcanoes were built, which have responded in a more rigid way to the transpressive and transtensive Middle to Upper Miocene deformation. In the Upper Miocene-Pliocene the whole belt was the scenario of extensive volcanic activity, both effusive and explosive, forming several stratovolcanoes, dome complexes with their related pyroclastic facies most of them with their emplacement tectonically controlled by NS and NE-SW structures, and received distal facies of regional ignimbrites such as the Salar Grande (10–12 Ma; Clavero et al., 1998; Naranjo et al., 2013b). During the Middle to Upper Miocene several phreatomagmatic vents, located in a dozen of different areas across the belt, previously unreported and matter of this paper, are spatially and temporarily related to the areas affected by HS hydrothermal alteration. Despite the lack of major structures in the regional maps published by Sernageomin (Naranjo et al., 2013a, 2013b; Villa et al., 2019), the volcanic vents as well as the magmatic feeders of the phreatomagmatic activity have been structurally controlled by local transpressive and transtensive tectonics, which do not generate major fault displacement but seem to play an

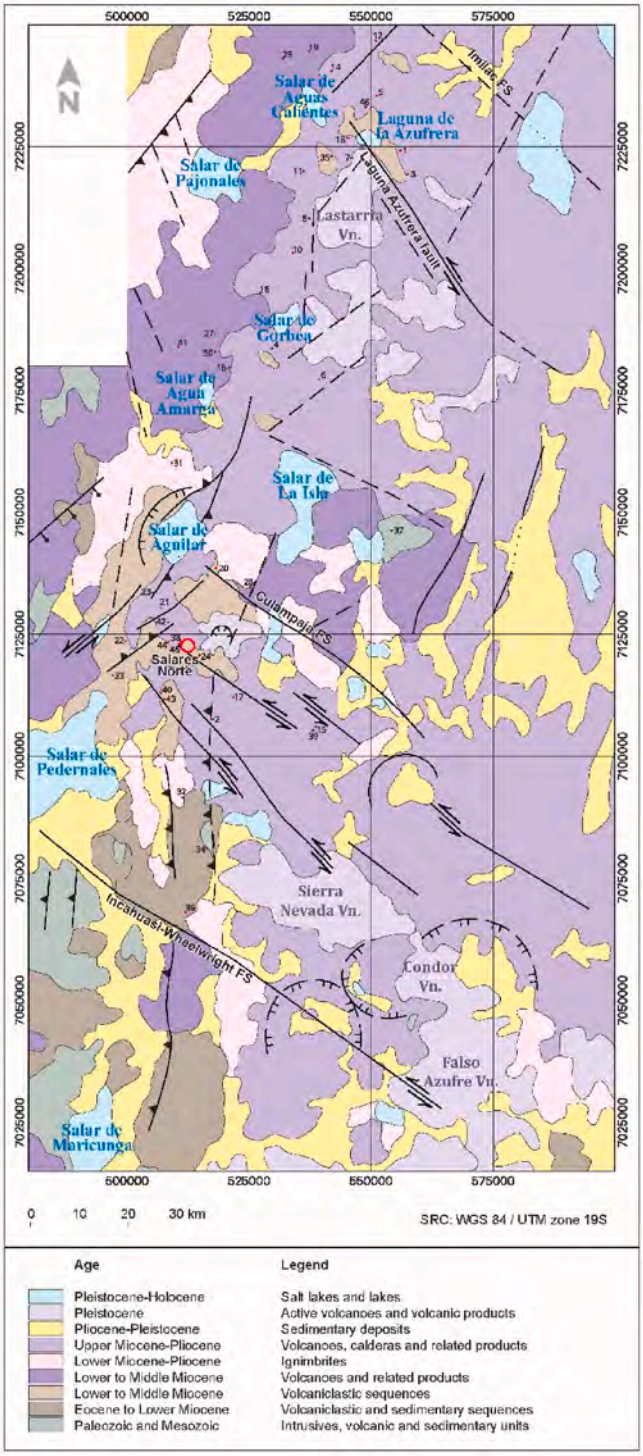


Fig. 4. Geologic framework of the Salares Norte Belt
Geologic and structural information compiled, simplified, and modified from Clavero et al. (1998, 2012), Cornejo et al. (1998, 2009), Naranjo et al. (2013a, 2013b, 2016, 2019), Rubiolo and Pereyra, 2003, Seggiaro et al. (2006, 2007), Tomlinson et al. (1999), Villa et al. (2019) and Zapettini (2001).

important role both in volcanic location and hydrothermal fluid circulation in the Middle to Upper Miocene.

Finally, in the Pleistocene the small-volume Chato Aislado explosive caldera formed in the central part of the area (Naranjo and Cornejo, 1992), synchronically with the activity of the Lastarria and Cordón del Azufre volcanoes (Naranjo et al., 2019b).

For a better understanding of the main geological, volcanological and tectonic features of the belt, we have subdivided its characterization into three main segments, from North to South: Laguna de la Azufrera-Salar de Aguas Calientes, Salar de Gorbea-Plato de Sopa, and Salares Norte.

4.2.1. Northern segment (Laguna de la Azufrera-Salar Aguas Calientes)

The northern segment is defined as the area located between the active volcanoes Llullaillaco on the north and Cordón del Azufre to the south (Fig. 5).

4.2.1.1. Volcanostratigraphy. The rocks cropping out in this northern segment of the Salares Norte belt are exclusively of volcanic and volcanoclastic origin (Fig. 4) with ages ranging from the Lower Miocene to the Pleistocene (Naranjo et al., 2013a,b; Villa et al., 2019). They can be grouped into four main units: i) pre-phreatomagmatic folded volcanoclastic sequences from the Lower Miocene; ii) volcanic rocks, mainly effusive, from the Middle to Upper Miocene; iii) tuffs, breccias, and subvolcanic intrusions associated with phreatomagmatic volcanism from the Upper Miocene to Pliocene, previously unrecognized in this area; and iv) post-phreatomagmatic volcanic rocks, effusive and explosive, Pliocene to Pleistocene in age.

The oldest rocks, Late Oligocene (?) to Lower Miocene in age, comprise a folded and faulted sequence up to 150 m thick, informally named in this study as the "Laguna de la Azufrera Sequence" (Fig. 6). The sequence consists of well-stratified to laminated layers, with centimeter to metric thicknesses of primarily volcanic rocks. These rocks are dominated by basaltic-andesite and silicic-andesite lavas, as well as subordinate dacitic lavas and domes. The sequence also includes massive and laminated pumice-rich, pumice-lithic, and scoriaceous pyroclastic rocks, along with dacitic pyroclastic breccias. The basaltic-andesite lavas are porphyritic with plagioclase, pyroxene, occasional amphibole, and/or olivine phenocrysts, in a trachytic to vesicular matrix. Some flows exhibit characteristic large olivine phenocrysts (<2 cm) and peridotitic nodules with olivine, garnet, and plagioclase. The silicic andesite to dacitic lavas are porphyritic with plagioclase, pyroxene, sanidine, and/or quartz and/or amphibole phenocrysts, in an aphanitic to vitreous groundmass. The dacitic domes contain plagioclase, biotite,

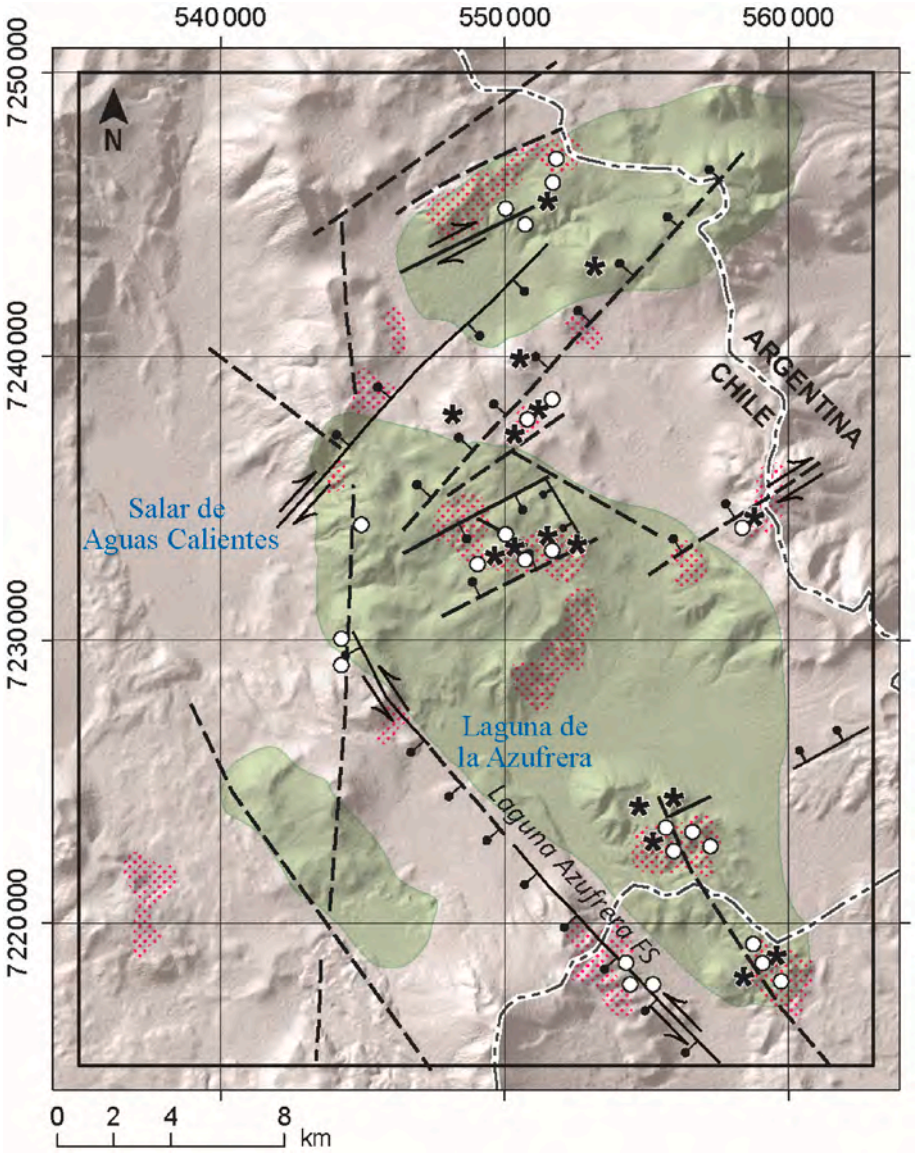


Fig. 5. Volcano-tectonic setting of the northern segment of the Salares Norte belt
Exogenous domes (stars), maar-diatreme systems (white circles) and hydrothermally altered areas (red dots) are shown, as well as main faults and inferred extension of Upper Oligocene-Lower Miocene volcanoclastic sequences (green shaded polygons).

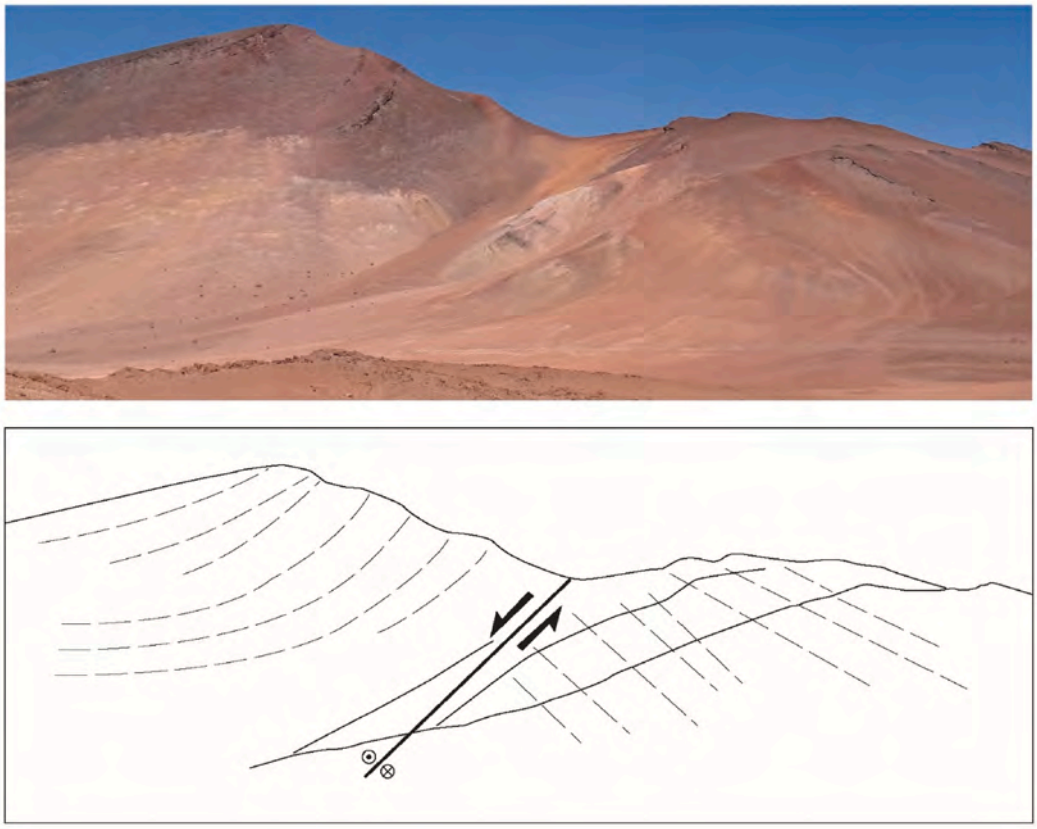


Fig. 6. Upper Oligocene-Lower Miocene folded and faulted volcanoclastic sequence
Photograph towards the West from Laguna de la Azufrera area, showing the folded layers of the Laguna de la Azufrera volcanoclastic sequence associated to a sinistral-normal fault.

amphibole, quartz, and sanidine phenocrysts in a glassy to flow-banded matrix, with varying vesicles content.

The pyroclastic-epiclastic facies of Laguna de la Azufrera sequence consists of individual layers ranging from 8 to 120 cm thick. It is composed of ash to medium-fine lapilli pumice tuffs, well-sorted and massive, resulting from fallout deposits. There are also well-laminated medium to coarse ash tuffs, rich in biotite and quartz crystal fragments within the matrix, formed by diluted pyroclastic density currents. The sequence includes massive, poorly sorted dacitic pyroclastic block-and-ash flow breccias, occasionally interbedded with laminated ash-cloud-surge ash tuffs. In some places, interbedded within the sequence there are epiclastic lahar layers, consisting of massive polymictic breccias with medium to coarse laminated sandstones interbedded, some of which are rich in rounded pumice fragments.

The volcanic rocks predating phreatomagmatic events mainly consist of lavas and domes with limited scoria-rich pyroclastic breccias. The lavas are silicic andesite in composition, with plagioclase and pyroxene phenocrysts in an aphanitic groundmass, occasionally displaying penetrative flow banding. The domes are primarily dacitic, showing folded flow banding, glassy and partly devitrified bands, and containing plagioclase, pyroxene, biotite, quartz, and/or sanidine phenocrysts, along with occasional xenocrysts of olivine, in a vitreous to vesicular

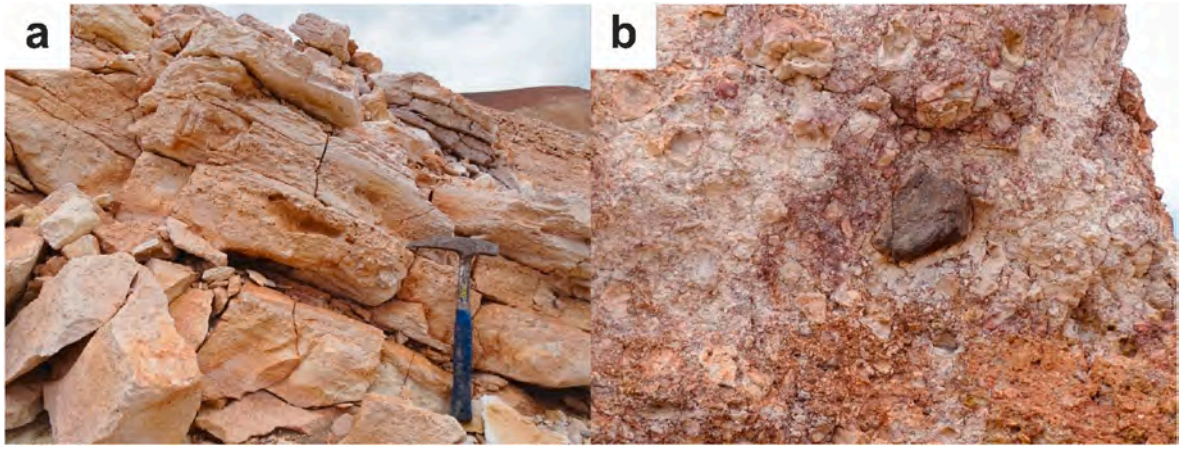


Fig. 7. Phreatomagmatic tuffs and breccias of the northern segment of the Salares Norte belt
a) Well-stratified and inclined hydrothermally-altered ash and lapilli phreatomagmatic tuffs. b) Lithic-rich massive and poorly-sorted phreatomagmatic breccia.

matrix. The scoria-rich pyroclastic breccias are monolithologic and massive, containing bombs up to 60 cm in diameter, dense andesitic-basaltic fragments in a coarse ash to lapilli scoria-rich matrix.

The rocks associated with phreatomagmatic volcanism mainly consist of pyroclastic rocks and, to a lesser extent, subvolcanic intrusions. The pyroclastic rocks include ash tuffs, lapilli tuffs, and tuff breccias, lithic to pumice-lithic, massive to well-stratified and finely laminated (Fig. 7a and b), with exposed thicknesses of up to 15 m. Stratified rocks are composed of individual layers with thicknesses of 0.5–8 cm, with variable strikes and dips, the latter ranging from sub-horizontal to 45°. In some areas, these rocks are deformed (syn-depositional deformation) due to the instability within the diatreme conduit, occasionally containing dacitic lava blocks up to 1.8 m in diameter. The medium to coarse ash tuffs, massive to laminated, in some sectors, include remnants of juvenile pumice fragments, rounded dense juvenile fragments, and lithic fragments in a fine ash matrix rich in clay and fractured plagioclase and quartz crystals. The fine lapilli tuffs consist of dense juvenile fragments, subrounded to subangular lithic fragments, occasional larger lithics and juvenile blocks, some with puzzle-type fracturing, in a silicified fine ash matrix with disseminated crystalline jarosite. The tuff breccias consist of subangular to subrounded polylithologic lithic fragments with relict porphyritic texture and subrounded juvenile fragments with wavy edges, in a fine to medium ash matrix replaced by quartz-jarosite, some containing plagioclase crystals. Scarce small-volume subvolcanic intrusions, spatially and genetically associated with maar-diatreme systems (Fig. 5), are primarily silicic andesite to dacitic in composition. They contain altered plagioclase and oxidized pyroxene phenocrysts in a groundmass ranging from microcrystalline rich in plagioclase to aphanitic.

The volcanic post-phreatomagmatic events rocks in this segment of Salares Norte belt mainly correspond to lavas, lava domes, and domes, occasionally filling the partially eroded crater depression of maar-diatreme systems. Additionally, a subordinate dacitic pyroclastic sequence is present. These lavas, lava domes, and domes are andesitic-siliceous to dacitic in composition, preserving some primary structures such as penetrative jointing, folded flow banding (non-magmatic folding), and, in some areas, discontinuous bands with varying degrees of vesicularity. They also exhibit porphyritic texture, with scarce phenocrysts of plagioclase, pyroxene, biotite, sanidine, and/or quartz in an aphanitic to glassy and slightly vesicular groundmass. The pyroclastic rocks are massive, up to 25 m thick, monolithologic, dacitic in composition, and are associated with block-and-ash flows resulting from partial dome collapses. Younger volcanic rocks and pyroclastic deposits associated to the active Lastarria and Cordón del Azufre volcanoes, as well as some Pleistocene ignimbrites, are also located in this segment of the belt, whose products partially cover some of the hydrothermally altered phreatomagmatic centers.

4.2.1.2. Phreatomagmatic volcanism. In this northern segment of the region, at least 6 areas have been identified where rocks of phreatomagmatic origin are exposed (Fig. 5). These rocks cut across and partially cover the rocks of the Laguna de la Azufrera Sequence and/or Upper Miocene volcanic products. They are, in turn, partially covered by Pliocene domes and lavas. All these sectors are closely related to HS hydrothermal alteration and are locally affected by normal-sinistral and normal-dextral faults.

In the Northern area (one cluster), the rocks are associated with at least 4 maar structures, probably controlled by NE-SW oriented faults, some of which are spatially associated with posthumous domes and small subvolcanic intrusives.

In the Central area (two clusters), the phreatomagmatic rocks may be associated to at least 6 maar-diatreme systems, spatially related with areas affected by HS hydrothermal alteration. These systems are controlled by sinistral-normal fault structures, oriented NE-SW. Sometimes, they are crowned by posthumous or late phreatomagmatic dacitic domes, aligned in the same direction and located at the edges of the maars. There are also a series of small subvolcanic intrusive bodies spatially associated both to the phreatomagmatic structures and the hydrothermal alteration.

In the Southern area, three clusters with outcrops of phreatomagmatic pyroclastic rocks affected by hydrothermal alteration are recognized. These rocks are primarily emplaced in folded rocks of the Laguna de la Azufrera Sequence and, to a lesser extent, in Upper Miocene volcanic rocks. They are partially covered by a series of late Pliocene lavas and domes. In these sectors, the rocks may be related to at least 10 maar-diatreme systems, with complex contact relationships between them. Some are nested, others are superimposed, or located on the edges of older ones within the same phreatomagmatic volcanic cycle. The orientation of the maar-diatreme systems is essentially NW-SE, although there are also less significant tectonic controls in other directions.

4.2.1.3. Age and hydrothermal alteration. The phreatomagmatic pyroclastic rocks are moderately to strongly affected by hydrothermal alteration, mainly of argillic, advanced argillic, steam-heated, or goethite-hematite types. The areas affected by steam-heated alteration display remnants of silicified lithic fragments, some exhibiting vuggy silica alteration textures and abundant native sulfur. Locally, the subvolcanic intrusions contain cavities and veins filled with jarosite, native sulfur, and alunite. In contrast, the country rocks of the phreatomagmatic explosions are locally heavily fractured and affected by various degrees and types of hydrothermal alteration. Remnants of lavas within these rocks exhibit silicification and/or alteration to goethite-hematite, while the pyroclastic breccias show signs of steam-heated alteration (clays and native sulfur).

Villa et al. (2019) present a series of geochronological data from pre-phreatomagmatic volcanic rocks near the explosive centers, unaffected by hydrothermal alteration (Fig. 4), indicating an age range between 6.46 and 7.76 million years. On the other hand, Barrick Exploraciones (2002 in SIGEX, Sernageomin) provides an age of hydrothermal alteration in one of the maar fields in this northern segment, just north of Laguna de la Azufrera (Ar–Ar in alunite), of approximately 4.9 million years (Table 1). Given the contact relationships and ages published by both these authors and Naranjo et al., 2013a,b in pre- and post-phreatomagmatic rocks and alteration events, it is suggested that the maar fields in this sector likely formed in the range between 6 and 4 Ma, while at least one of the hydrothermal alteration events occurred around 4.9 Ma (Pliocene).

4.2.2. Central segment (Salar de Gorbea-Plato de Sopa)

The central segment is defined as the area located just south of the active volcanic area of Cordón del Azufre to the north, and Salar de la Isla to the south (Fig. 8).

4.2.2.1. Volcanostratigraphy. Stratigraphically, in this sector, volcanic and volcanoclastic rocks have been identified, with ages ranging from the Lower Miocene to the Pliocene according to the available regional data (Naranjo et al., 2013a, 2013b). These rocks can be grouped into three main units (Fig. 10): i) gently deformed volcanoclastic to volcanic sequences from the Lower to Middle Miocene predating phreatomagmatic events; ii) tuffs and breccias of phreatomagmatic origin probably associated with two periods of this type of volcanism in the Middle Miocene and the Upper Miocene to Pliocene; and iii) primarily effusive volcanic rocks and, to a lesser extent, explosive ones predating and postdating phreatomagmatic events from the Upper Miocene to Pliocene.

The volcanoclastic sequences, shown as green shaded areas in Fig. 8, consist of sedimentary and volcanic layers, both effusive and explosive, of continental origin, with facies variations, some with a greater predominance of epiclastic and pyroclastic sedimentary components, and

Table 1
Selected regional geochronological data numbered in Fig. 4.

N° Fig. 4	Sample Code	Unit	UTM East	UTM North	Lithology	Method	Mineral	Age ± 2σ error	Reference
1	560067837	n.a.	555966	7224208	Fresh rock	U–Pb	Zircon	2.85 ± 0.05	(Inversiones Barrick Conosur Ltda, 2022)
2	560082181	n.a.	517528	7107580	Unknown	U–Pb	Zircon	3.54 ± 0.04	(ENAMI, 2018)
3	GN-583	Upper Miocene-Lower Pliocene volcanoes	557491	7219356	Andesite scoria	K–Ar	Whole-rock	3.8 ± 0.9	(Naranjo and Cornejo, 1992)
4	GN-259	Upper Miocene-Lower Pliocene volcanoes	529700	7183665	Andesite	Ar–Ar	hornblende	4.12 ± 0.12	Naranjo et al., 2013a,b
5	V260317-6	Upper Miocene-Lower Pliocene volcanoes	551166	7235473	Dacite	Ar–Ar	Groundmass	4.16 ± 0.04	Villa et al. (2019)
6	GN-659	Upper Miocene-Lower Pliocene volcanoes	539389	7177348	Lava	K–Ar	Whole-rock	4.9 ± 0.5	(Naranjo and Cornejo, 1992)
7	GN-126	Upper Miocene-Lower Pliocene volcanoes	546105	7222628	Andesite	K–Ar	Whole rock	5.3 ± 0.4	(Naranjo and Cornejo, 1992)
8	230511–10	Upper Miocene-Lower Pliocene volcanoes	537363	7210208	Lava	Ar–Ar	Groundmass	5.37 ± 0.03	Naranjo et al., 2013a,b
9	SO-465	Upper Miocene-Lower Pliocene volcanoes	542471	7254013	Dacite	K–Ar	Whole rock	5.6 ± 0.9	(Gardeweg et al., 1993)
10	GN-185	Upper Miocene-Lower Pliocene volcanoes	534038	7203122	Dacite	Ar–Ar	Hornblende	5.74 ± 0.18	Naranjo et al., 2013a,b
11	GN-36	Upper Miocene-Lower Pliocene volcanoes	536187	7219990	Andesite	K–Ar	Whole-rock	6.1 ± 0.3	(Naranjo and Cornejo, 1992)
12	C090117-2	Upper Miocene-Lower Pliocene volcanoes	550996	7246644	Dacite	Ar–Ar	Groundmass	6.67 ± 0.04	Villa et al. (2019)
13	GN-120A	Upper Miocene-Lower Pliocene volcanoes	545251	7226751	Lava	K–Ar	Whole rock	7.8 ± 0.5	(Naranjo and Cornejo, 1992)
14	V130517-5	Upper Miocene-Lower Pliocene volcanoes	541907	7240523	Andesite	Ar–Ar	Groundmass	8.47 ± 0.13	Villa et al. (2019)
15	GP-57	Upper Miocene Lower Pliocene volcanoes	538771	7106073	Dacitic dome	U–Pb	Zircon	9.6 ± 0.1	This study
16	GN-412A	Middle to Upper Miocene volcanoes	520929	7179588	Andesite	K–Ar	Whole-rock	14.5 ± 0.9	(Naranjo and Cornejo, 1992)
17	GCo-310	Middle to Upper Miocene volcanoes	521857	7112026	Basaltic andesite	K–Ar	Whole-rock	10.4 ± 0.4	Clavero et al. (1998)
18	GN-197	Middle to Upper Miocene volcanoes	527298	7194953	Andesite	K–Ar	Whole-rock	12.8 ± 0.7	(Naranjo and Cornejo, 1992)
19	V230317-3	Middle to Upper Miocene volcanoes	537368	7244604	Andesite	Ar–Ar	Groundmass	13.06 ± 0.07	Villa et al. (2019)
20	GN-400	Middle Miocene volcaniclastic sequence	518233	7138584	Andesite lava	K–Ar	Whole-rock	13.2 ± 0.7	(Naranjo and Cornejo, 1992)
21	AG-113	Middle Miocene volcaniclastic sequence	507032	7130471	Andesite lava	U–Pb	Zircon	13.6 ± 0.3	GoldFields Salares Norte SpA, 2020
22	n.a.	Middle Miocene volcaniclastic sequence	499804	7123589	n.a.	K–Ar	Whole rock	14.1 ± 0.5	(Cornejo et al., 1993)
23	AG-139	Middle Miocene volcaniclastic sequence	505292	7133498	Rhyolitic tuff	U–Pb	Zircon	14.7 ± 0.3	GoldFields Salares Norte SpA, 2020
24	AG-223	Middle Miocene volcaniclastic sequence	514827	7120697	Dacite	U–Pb	Zircon	15.7 ± 0.2	GoldFields Salares Norte SpA, 2020
25	V150517-7A	Lower to Middle Miocene volcanoes	531981	7243078	Andesite	Ar–Ar	Groundmass	15.00 ± 0.06	Villa et al. (2019)
26	C270516-3	Lower to Middle Miocene volcanoes	538063	7260352	Dacite	Ar–Ar	Whole-rock	15.71 ± 0.04	Villa et al. (2019)
27	GN-371	Lower to Middle Miocene volcanoes	517996	7186564	Lava	K–Ar	Whole-rock	17.3 ± 0.7	(Naranjo and Cornejo, 1992)
28	GN-685	Lower to Middle Miocene volcanoes	525280	7134569	Andesite	K–Ar	Whole rock	19.2 ± 0.9	(Naranjo and Cornejo, 1992)
30	200511-1C	Lower to Middle Miocene ignimbrites	518085	7182931	Pumice	Ar–Ar	Biotite	15.6 ± 1.1	Naranjo et al., 2013a,b
31	GN-571A	Lower to Middle Miocene ignimbrites	509226	7160112	Ignimbrite	K–Ar	Biotite	17.7 ± 1.4	(Naranjo and Cornejo, 1992)
32	GCO-391	Lower to Middle Miocene ignimbrites	511294	7091492	rhyolitic ignimbrite	Ar–Ar	Whole rock	18.361 ± 0.203	Clavero et al. (1998)
33	n.a.	Upper Oligocene-Lower Miocene volcaniclastic sequence	497061	7116525	n.a.	K–Ar	Biotite	20.5 ± 0.7	(Cornejo et al., 1993)
34	JCO-55.8	Upper Oligocene-Lower Miocene volcaniclastic sequence	516433	7081203	Rhyodacitic ignimbrite	K–Ar	Biotite	22.0 ± 0.9	Clavero et al. (1998)
35	GN-101A	Upper Oligocene-Lower Miocene volcaniclastic sequence	541966	7223036	Andesite	K–Ar	Whole rock	23.7 ± 0.9	(Naranjo and Cornejo, 1992)

(*continued on next page*)

Table 1 (*continued*)

N° Fig. 4	Sample Code	Unit	UTM East	UTM North	Lithology	Method	Mineral	Age ± 2σ error	Reference
36	JCO-53.8	Upper Oligocene-Lower Miocene volcaniclastic sequence	511966	7068007	Dacitic ignimbrite	K–Ar	Biotite	25.7 ± 1.7	Clavero et al. (2012)
37	180511–24	Paleozoic basement	554252	7146257	Dacite	U–Pb	Zircon	265.1 ± 2.6	Naranjo et al., 2013a,b
38	AG-258	Phreatomagmatic volcanism	510766	7123684	Phreatomagmatic lapilli tuff	U–Pb	Zircon	9.1 ± 0.2	GoldFields Salares Norte SpA, 2020
39	GP-28	Phreatomagmatic volcanism	538162	7105279	Phreatomagmatic pumiceous lapilli tuff	U–Pb	Zircon	9.6 ± 0.1	This study
40	AG-304	Phreatomagmatic volcanism	507060	7112891	Phreatomagmatic tuff breccia	U–Pb	Zircon	13.6 ± 0.1	GoldFields Salares Norte SpA, 2020
41	7001428	Hydrothermal alteration	510533	7184055	Polymictic breccia with silica-alunite matrix	Ar–Ar	Alunite	17.37 ± 0.39	Newcrest Chile Spa, 2022
42	A3DD026	Hydrothermal alteration	508533	7127437	Altered andesitic lava	Ar–Ar	Natroalunite	14.32 ± 0.09	Gold Fields Salares Norte SpA, 2020
43	AG-316	Hydrothermal alteration	507541	7111933	Altered phreatomagmatic tuff	Ar–Ar	Jarosite	11.84 ± 0.14	Gold Fields Salares Norte SpA, 2020
44	AG-292	Hydrothermal alteration	508446	7123448	Phreatomagmatic breccia	Ar–Ar	Jarosite	6.94 ± 0.10	Gold Fields Salares Norte SpA, 2020
45	SN-DAT-05	Hydrothermal alteration	510711	7123016	Altered phreatomagmatic tuff	Ar–Ar	Alunite	5.35 ± 0.19	Santos (2014)
46	560067767	Hydrothermal alteration	548900	7233058	Altered phreatomagmatic breccia, silica-jarosite alteration overprinted by alunite K	Ar–Ar	Alunite	4.9 ± 0.2	(Inversiones Barrick Conosur Ltda, 2022).

others with a predominance of effusive volcanic components. The sequences are subhorizontal to gently folded to steeply dipping, with inclinations of up to 35–40° (Fig. 9a). The epiclastic-pyroclastic sequences, up to 80 m thick, are composed of layers of variable thicknesses between 10 and 150 cm of pyroclastic tuffs and breccias interbedded with conglomerates, sedimentary breccias, and sandstones. The tuffs range from ash to fine lapilli pumice-lithic, massive to well-stratified (Fig. 9b) and contain subrounded silicified pumice and/or lithic fragments contained in a fine to medium ash matrix, locally silicified. The sedimentary layers correspond to medium to coarse grained laminated sandstones, with lenses and low-angle parallel and cross-stratification, fine conglomerates with rounded silicified lithic fragments and/or subrounded pumice fragments contained in a fine to medium sand matrix replaced by silica, and occasional levels of polymictic massive sedimentary breccias with subrounded to rounded fragments, interbedded with finely laminated sandstones. These characteristics indicate that they probably correspond to lahars with their dense (debris flow) and more diluted (flooding and/or tail) facies. The pyroclastic breccias are essentially associated to block-and-ash flows and to scoria flows. The block and ash type breccias reach individual thicknesses of up to 15 m, have dacitic composition and are monolithological, essentially massive, with scarce and thin intercalated layers of ash-cloud-surge type ash layers. They contain blocks up to 60 cm in diameter with prismatic jointing in a matrix of medium ash. The blocks have porphyritic texture with plagioclase, sanidine, pyroxene, and quartz phenocrysts in a vitreous groundmass with some plagioclase and pyroxene microlites, with varying degrees of vesicle content. The scoria-rich pyroclastic breccias reach individual thicknesses of up to 12 m, they contain andesitic scoria fragments of up to 50 cm in diameter, occasionally with a cauliflower-like texture, in a matrix of medium to coarse ash.

The predominantly effusive volcanic sequences, reaching exposed thicknesses of up to 150 m, are composed of lava flows and domes. The lavas, up to 25 m in individual thickness, range in composition from silicic-andesite to dacitic. They present well-preserved primary features such as flow banding, autoclastic and/or vesicular bands. They have porphyritic texture with plagioclase, pyroxene, biotite, amphibole, quartz, and/or sanidine phenocrysts in an aphanitic to glassy groundmass. The domes are dacitic in composition with relict porphyritic texture with plagioclase, biotite, amphibole, pyroxene, quartz, and occasional sanidine phenocrysts, in a hematitized, argillized, or fresh groundmass. They locally present autoclastic breccias and internal structures like flow banding, partly folded, slabby fracturing, and/or lithophysae. In specific sectors of this segment, sequences of up to 50 m in thickness of basaltic-andesite lavas, up to 4 m thick, have been recognized within the effusive sequences. They show porphyritic texture with scarce phenocrysts of plagioclase, pyroxene, olivine, and occasional amphibole in an aphanitic to glassy, somewhat fluidal, groundmass, with spherical to oval vesicles.

The phreatomagmatic rocks associated with maar-diatreme systems consist essentially of different types of pyroclastic rocks ranging from dacitic to rhyolitic compositions and, to a lesser extent, subvolcanic intrusive rocks ranging from silicic-andesite to dacitic compositions. The pyroclastic rocks include ash tuffs and lapilli tuffs, lithic to pumice-rich, massive to well-stratified. In some areas, they present several internal structures such as parallel lamination, trough cross-bedding, wavy bedding, and low-angle cross-stratification, load structures, and lenses, as well as highly variable strikes and dips (Fig. 9c and d), which can be associated to different internal sectors of a maar-diatreme system and, to a lesser extent, to external tuff ring facies (e.g. Lorenz, 2003; Valentine and White, 2012). Among their main lithologies are ash tuffs and fine lapilli tuffs, which consist of highly variable contents of polymictic lithic fragments, pumice fragments, laminated intra-clasts (clasts of laminated phreatomagmatic tuffs of previous explosions usually with undulated borders), and occasional glassy undulated fragments and puzzle-like lithics, within a plagioclase and quartz crystal fragments-rich ash matrix. In some areas, lithic fragments and/or the tuff matrix is slightly to strongly affected by hydrothermal alteration, such as silicification or quartz-alunite.

The subvolcanic intrusive rocks are of small volume and limited areal extent at surface. They are spatially associated with the identified phreatomagmatic centers, being emplaced mainly near the edges of these structures. They correspond to porphyritic rocks, dacitic to silicic-andesite in composition, with plagioclase, pyroxene, and/or sanidine phenocrysts in a dark gray aphanitic groundmass with plagioclase microlites In some areas, they present flow banding, vesicular texture, and/or oval mafic inclusions.

The post-phreatomagmatic volcanic rocks are represented by a series of domes and lava flows with large areal distribution, several of which were emplaced at the edges of maar structures or as partial infill of the maar crater depressions (Fig. 10). The lavas are silicic-andesite to dacitic in composition with plagioclase, pyroxene, quartz, and/or sanidine

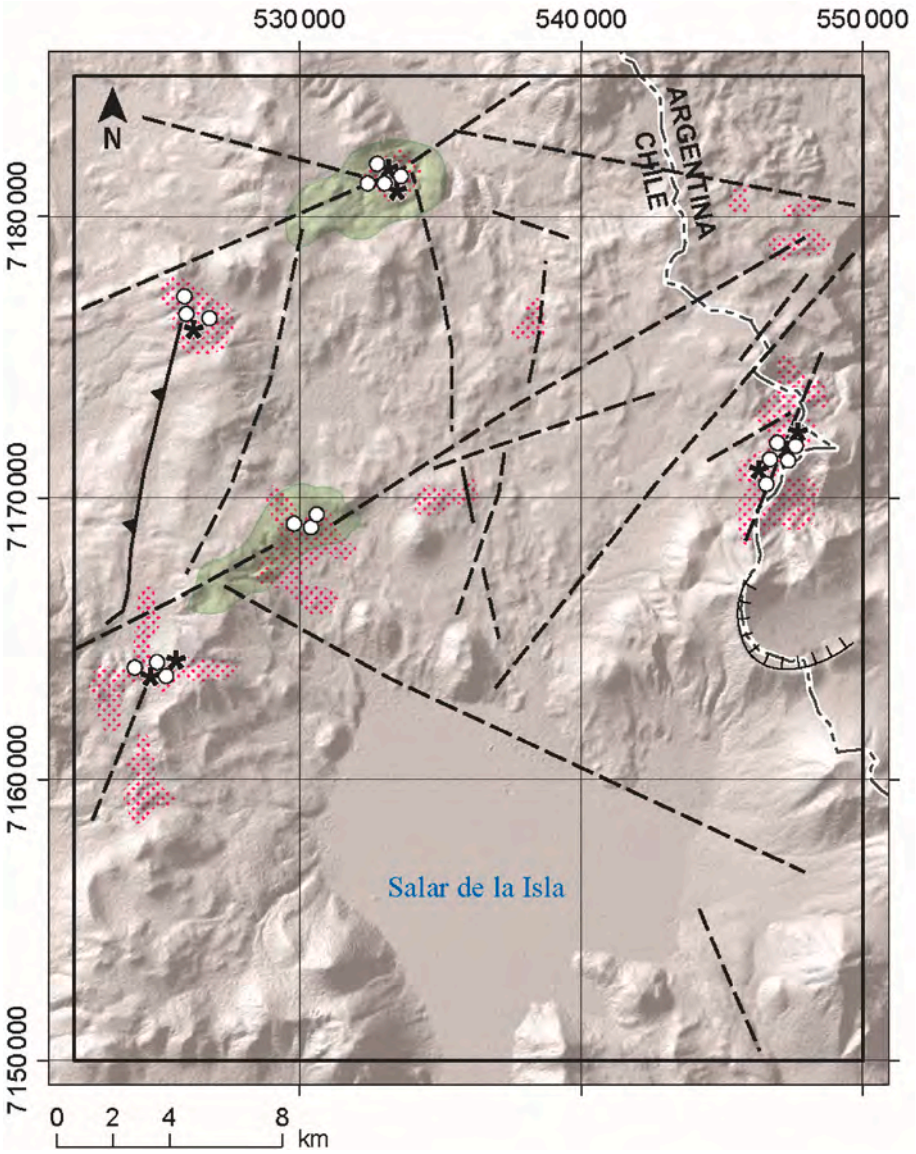


Fig. 8. Volcano-tectonic setting of the central segment of the Salares Norte belt.
Exogenous domes (stars), maar-diatreme systems (white circles) and hydrothermally altered areas (red dots) are shown, as well as main faults and inferred extension of Lower Miocene volcanoclastic sequences (green shaded polygons).

phenocrysts in a dense to aphanitic glassy groundmass. In some areas, alteration to smectite and/or hematite-goethite is recognized, in addition to vesicles of irregular morphology and/or autoclastic zones. The domes are mainly rhyodacitic to dacitic in composition and are composed of plagioclase, pyroxene, biotite, quartz, and/or sanidine phenocrysts in an aphanitic to glassy groundmass, slightly vesicular, locally showing folded flow banding as well as monolithologic autoclastic breccias.

4.2.2.2. Phreatomagmatic volcanism. In this central segment of the volcanic belt, phreatomagmatic rocks have been identified in at least four areas (Fig. 8). In these sectors, the petrographic and structural characteristics of the phreatomagmatic rocks have allowed to infer the existence of various maar-diatreme type structures. These are arranged as small clusters of 3 to more than 7 maar-diatreme structures (Fig. 8), located within structurally controlled zones, partially nested or with cross-cutting relationships, usually spatially associated to exogenous domes.

The inferred morphology of the paleocraters varies from subcircular to elliptical, the latter having elongated major axes according to the local stress regime at the time of formation. The highest occurrence of maars in this segment is found close to the Chile-Argentina border, where at least 7 maar-diatreme structures have been identified with complex contact relationships among them (nested, coalescent, and isolated). These structures are aligned in an approximately 4 km-long and NNE-SSW-oriented strip.

4.2.2.3. Age and hydrothermal alteration. The maar fields identified in this area are partially to almost completely affected by various types and degrees of HS epithermal alteration. The phreatomagmatic tuffs show evidence of multiple explosive events, partly contemporaneous with the circulation of active hydrothermal fluids which indicate, depending on the sector, the occurrence of at least 2 or 3 hydrothermal alteration events. The fluid circulation associated to these hydrothermal events was concentrated primarily in the phreatomagmatic rocks and in the most permeable levels of the surrounding country rock adjacent to the explosive structures, such as pyroclastic, epiclastic, or autoclastic facies of lavas and domes.

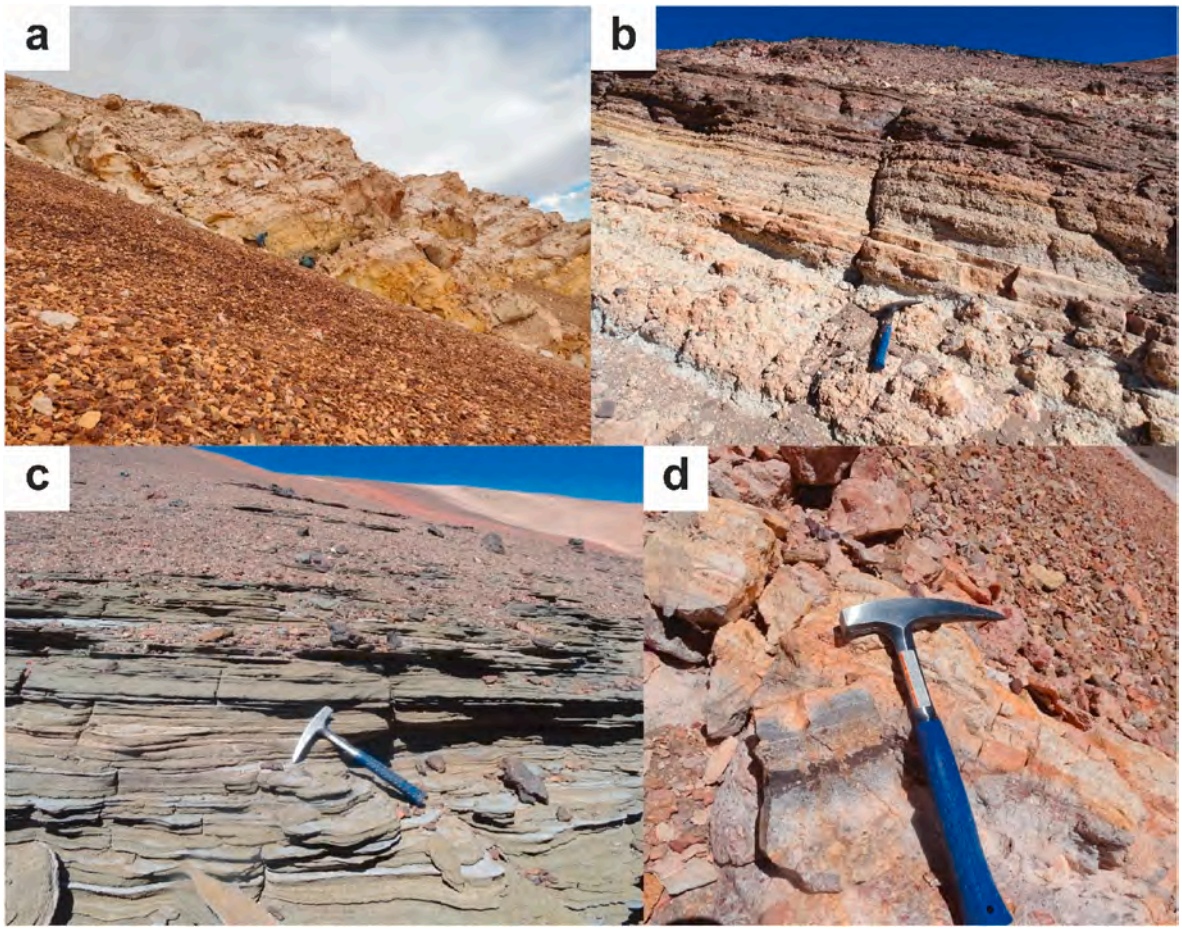


Fig. 9. Lower Miocene folded volcanoclastic sequences (a and b) and phreatomagmatic rocks (c and d) in the central segment of the Salares Norte belt.
a) Tilted epiclastic-pyroclastic sequence up to 70 m thick. b) Detail of a folded pyroclastic sequence formed by dacitic to rhyodacitic pyroclastic layers, both fallout and pyroclastic density current in origin. c) Subhorizontal well-stratified ash and fine-lapilli tuff layers associated to preserved maar tuff rings. d) Load structure within inclined well-stratified ash and lapilli phreatomagmatic tuffs.

The main types of hydrothermal alteration recognized in these rocks correspond to silicification (of different types), quartz-alunite, silica-jarosite, argillic, steam-heated, vuggy silica, and/or opal. The occurrence of several alteration events contemporaneous with the phreatomagmatic explosions is evidenced not only by the close spatial relationship between these volcanic structures and the areas affected by alteration but also by the coexistence, in breccias and phreatomagmatic tuffs, of fragments with various types of hydrothermal alteration. These include silicified fragments, fragments affected by quartz-alunite, fragments altered to jarosite and/or fragments with vuggy silica, sometimes included in an altered matrix to quartz-alunite.

There are few published ages of hydrothermal alteration to date in this segment, located towards the western part of the strip in sectors where the occurrence of phreatomagmatic volcanism has not been identified. These ages indicate the occurrence of alteration events in the Lower Miocene (approximately 17 Ma). However, there are some ages in volcanic rocks near some maar fields affected by HS-type epithermal alteration. These suggest that some of these alteration events may have occurred in the Upper Miocene-Pliocene, between 10 and 3 Ma (Fig. 4; Table 1).

4.2.3. *Southern segment (Salares Norte district)*

The southern segment is defined as the area located just south of the Salar de la Isla are to the north, and the east of Salar de Pedernales to the south (Fig. 11), which corresponds to the area known as the Salares Norte District.

4.2.3.1. Volcanostratigraphy. The geology of the southern segment comprises rocks and deposits with ages ranging from the Early Miocene to the Pleistocene-Holocene, where stratified units from the Early Miocene to the Middle Miocene, volcanic rocks and deposits from the Early Miocene to the Pleistocene, and phreatomagmatic rocks associated with at least three periods of explosive volcanism of this type, along with their associated subvolcanic intrusions, occur between the Middle Miocene (ca. 16 Ma) and the Upper Miocene (8–9 Ma). All these geological units represent at least seven relevant periods of magmatic-volcanic activity in the area.

4.2.3.2. Early to Middle Miocene. The oldest units that outcrop in this segment of the Salares Norte Belt correspond to an Early Miocene volcanic sequence, including the Río Frío and Pajonales ignimbrites of equivalent age, and an explosive volcanic sequence from the Early to Middle Miocene with little extension. The Early Miocene volcanic sequence, up to 150 m thick, locally known as the Infieles Sequence, outcrops as a north-south to NNE-SSW-oriented strip near the Infieles Salar. It exhibits folding with long-wavelength and low-amplitude folds, oriented N–S and NW-SE, and is affected by sinistral strike-slip faults. This sequence consists of lavas ranging from dacitic to andesitic compositions, pumice-rich moderately to strongly welded pumice-lithic lapilli tuffs, and dacitic pyroclastic block and ash flow type breccias. The Río Frio and Pajonales ignimbrites are dacitic tuffs, partly welded, restrictedly exposed to the northern part of the segment and cut by a NW-SE-trending dextral strike-slip fault (associated with the Culampaja Fault System). The fine ash rhyolitic tuffs of the Pajonales Ignimbrite

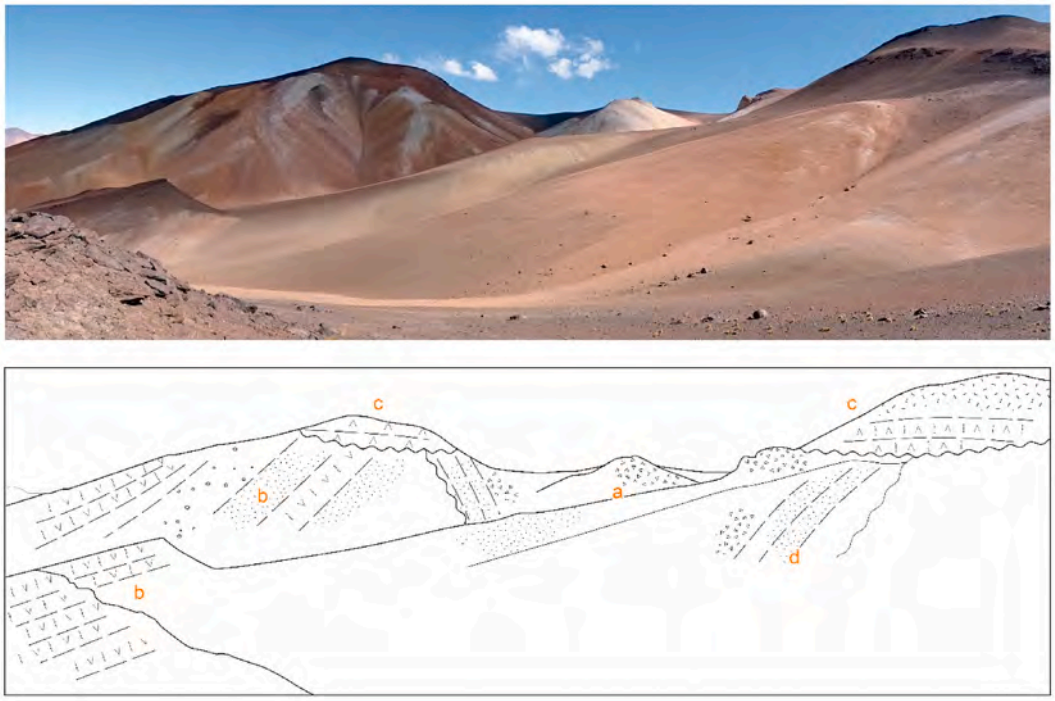


Fig. 10. View towards the North of hydrothermally altered phreatomagmatic centers in the northern part of the central segment
a) Phreatomagmatic pyroclastic breccias; b) Folded volcanoclastic sequence; c) Post-phreatomagmatic lavas and domes; d) Phreatomagmatic stratified tuffs.

form the core of a large plunging anticline associated with Middle Miocene deformation on the northeastern part of the segment. The Early to Middle Miocene volcanic sequence, crops out on the southern edge of the area close to the Tres Puntas volcano, and corresponds to a surtseyan-type succession of finely laminated and continuous ash and fine lapilli tuffs, locally folded with limb angles of up to 40° and NNE-oriented axes.

4.2.3.3. Middle Miocene. During this period, at least three small tectonically controlled volcano-sedimentary basins formed, diachronous in their development. The earliest, most extensive, and long-lived volcano-sedimentary sequence in the Middle Miocene in this segment is locally known as the Salares Norte Sequence. It consists of up to 180 m thick well-stratified sequence with volcanic and, subordinately, sedimentary rocks. It mainly outcrops in a NW-SE-oriented strip, covering more than 60 km^2, in the central part of the segment, with ages ranging from ca. 16 to 13 Ma. These rocks unconformably overlie rocks from the Early Miocene volcanic sequences and overlap in part with the also Middle Miocene Aster 2 Sequence. The rocks in this sequence are locally cut and partially covered by phreatomagmatic products associated with the youngest recognized explosive phreatomagmatic event in this segment (Upper Miocene). The rocks are moderately to heavily affected by alteration, varying from subhorizontal to locally tilted (30–35°) and faulted. The layers consist primarily of andesitic to basaltic-andesite lavas, dacitic block and ash flow type pyroclastic breccias, and andesitic scoriaceous pyroclastic breccias (Fig. 12a). Subordinately, the sequence contains interbedded fine to coarse sandstones, conglomeratic sandstones, and brecciated conglomerates, some of which contain rounded pumice fragments, indicating a significant fluvial-alluvial epiclastic component (Fig. 12b). Locally, progressive unconformities occur in alluvial facies close to major faults controlling the basin (Fig. 12c), indicating the synchronicity of deposition with tectonic activity that generated the basin. These rocks represent the products of basaltic andesite to dacite stratovolcanoes whose activity was synchronic with a transtensional tectonic period, which may have favored the formation of at least one sedimentary-pyroclastic depocenter oriented NW-SE (Salares Norte Basin). This basin would have deepened toward the NW and gradually shallowed toward the SE, where subaerial volcanic facies predominate.

Overlapping with the oldest phase of the Salares Norte basin, a volcano-sedimentary sequence locally named as Aster 2 Sequence formed in the northwestern sector of the segment, with ages between ca. 15 and 14 Ma. It consists of gently folded pyroclastic-epiclastic rocks up to 300 m thick, with scarce dacitic lavas. The sequence crops out as a N–S to NNW-SSE-oriented strip more than 14 km long and 6–8 km wide. In some places, the sequence is cut and/or overlaps with phreatomagmatic products associated with the oldest recognized event of this type in this part of the belt. It is common for these rocks to be affected by long-wavelength and low-amplitude folds with main axes oriented N–S to NNW-SSE. In some sectors, they also exhibit penetrative fracturing associated with normal and strike-slip faults oriented NW-SE and NE-SW. The sequence consists of fine to coarse sandstones, fine, medium, and coarse conglomerates, and some limy levels. Some of them contain rounded pumice fragments, indicating a significant fluvial-alluvial epiclastic component (Fig. 12d and e). These rocks result from the erosion of high topographic features uplifted by the Early Miocene compressive phase and synchronous with the volcanic products of basaltic andesite and dacite stratovolcanoes. The basin may have had its deepest part to the NW and gradually shallowed toward the SE, where subaerial volcanic facies predominate.

Cutting across and overlaying the Aster 2 and Salares Norte sequences, a series of small phreatomagmatic centers have been identified in the NW sector of the segment, with ages between 14 and 15 Ma. Some of the pyroclastic rocks belonging to these explosive centers are cut by ENE-WSW-trending normal faults. These rocks consist of ash-rich tuffs and lapilli tuffs, pumice-rich and pumice-lithic-rich, massive to stratified and laminated, with variable dips from gentle to 45°, which can be associated to different facies within a maar-diatreme system, including the lower non-stratified maar conduit, the upper stratified maar and, locally to the external tuff ring facies (e.g. Lorenz, 2003; Ross et al., 2017; Droguett et al., 2019). The coarser tuffs often contain abundant rounded intra-clasts of tuffs (fragments of previous phreatomagmatic

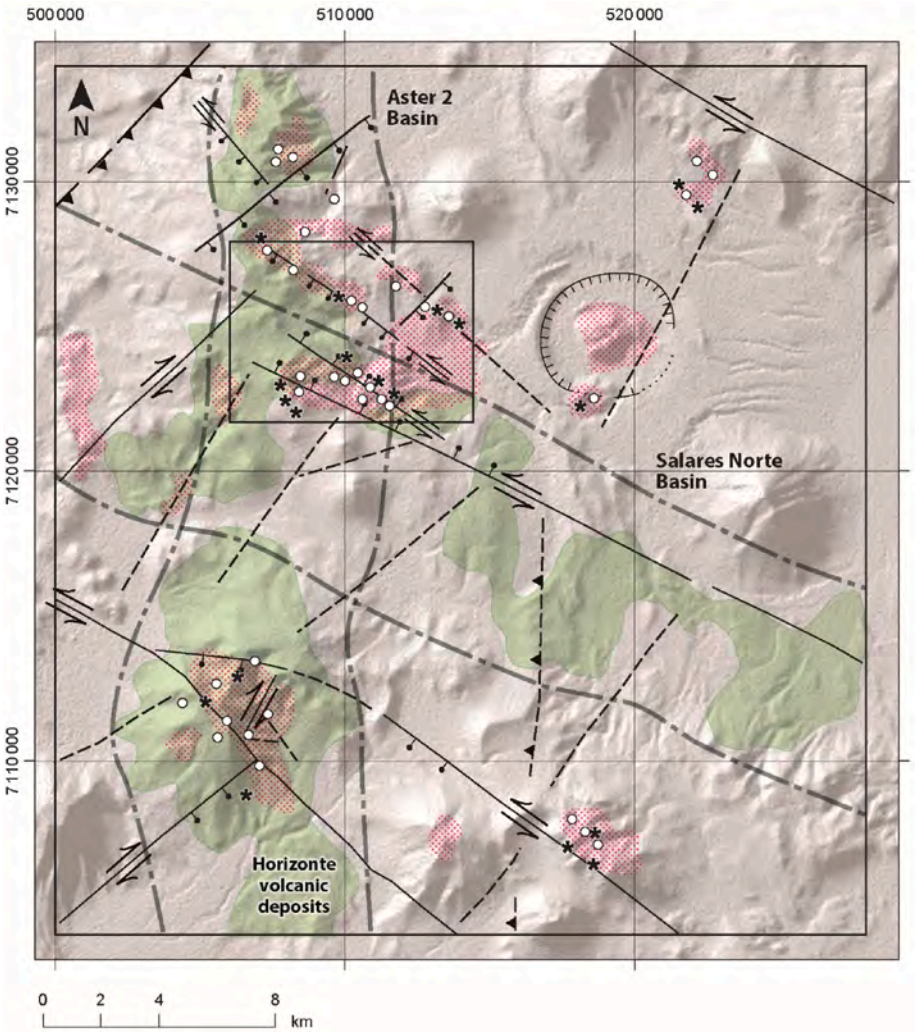


Fig. 11. Volcano-tectonic setting of the southern segment of the Salares Norte belt
Exogenous domes (stars), maar-diatreme systems (white circles) and hydrothermally altered areas (red dots) are shown, as well as main faults and inferred extension of Lower Miocene volcanoclastic sequences (green shaded polygons). Black rectangle shows the detail area included in Fig. 15.

explosions) and silicified porphyritic fragments, within a hydrothermally altered ash matrix (quartz-alunite, argillic and steam-heated).

Partially overlapping with the latest phase of the Salares Norte basin, in the southernwestern part of the segment, a predominantly volcanic sequence formed between 14 and 12 Ma, which forms a series of outcrops arranged as a north-south-oriented strip, up to 8 km long with an estimated thickness of approximately 200 m. These rocks, locally known as Horizonte Sequence interfingers with rocks from the Salares Norte Sequence and are spatially and temporally associated with phreatomagmatic rocks and hydrothermally altered areas of the same age in the same sector. They consist mainly of silicic-andesite lavas, dacitic block and ash flow type pyroclastic breccias, lapilli tuffs, and moderately welded pumice-rich breccias. Subordinately, they contain dacitic to rhyodacitic lavas and domes. This sequence is affected by strike-slip and mixed strike-slip-normal faults, oriented NW-SE, NNW-SSE, and NE-SW. These fault systems also generate a slight tilting of the layers, with dips of up to 30°. South of the Horizonte sector, pyroclastic breccias and partially welded tuffs belonging to this sequence show a low-amplitude, long-wavelength syncline. These rocks are gently folded, with main axes oriented NNW-SSE and limb inclinations of up to 35°. The absence of sedimentary facies identified in this sequence suggests that they are associated with mainly dacitic dome complexes and stratovolcanoes, with no significant epiclastic sedimentary depocenters near them.

The rocks of the Horizonte Sequence are cut, intruded, and partially covered by phreatomagmatic rocks, subvolcanic rocks and domes related to phreatomagmatic vents, in part synchronous with the terminal phase of volcanic activity that formed the sequence (ca. 12–13 Ma). The products of this phreatomagmatic volcanism, which can be associated with at least 8 maar-diatreme systems forming a NNE-SSW-oriented strip, are also spatially and temporally associated with the areas affected by intense HS-type hydrothermal alteration. The maars, in turn, form a strip at least 4 km long oriented NNW-SSE, associated with a series of sinistral-normal faults. The pyroclastic rocks of these maar-diatreme systems may be associated to lower un-stratified, upper stratified, and external subaerial tuff ring facies (e.g. Lorenz, 2003; Ross et al., 2017; Droguett et al., 2019).

Ignimbrites of distal origin to the Salares Norte District are located on the periphery of the district, such as the Upper Miocene (ca. 10–12 Ma) Salar Grande Ignimbrite (Naranjo, 1992). These tuffs, with thicknesses of up to 50 m, are subhorizontal to gently folded and overly the Early Miocene to Middle Miocene volcanoclastic sequences.

4.2.3.4. Upper Miocene. In the central part of the segment, where the Salares Norte Au–Ag Mine is under construction, a complex of domes and associated pyroclastic facies has been identified, locally known as the Brecha Principal Volcanic Complex, with ages ranging from 8 to 9 Ma. This complex was unconformably constructed above the gently folded rocks of the Salares Norte Sequence and consists of lavas, domes,

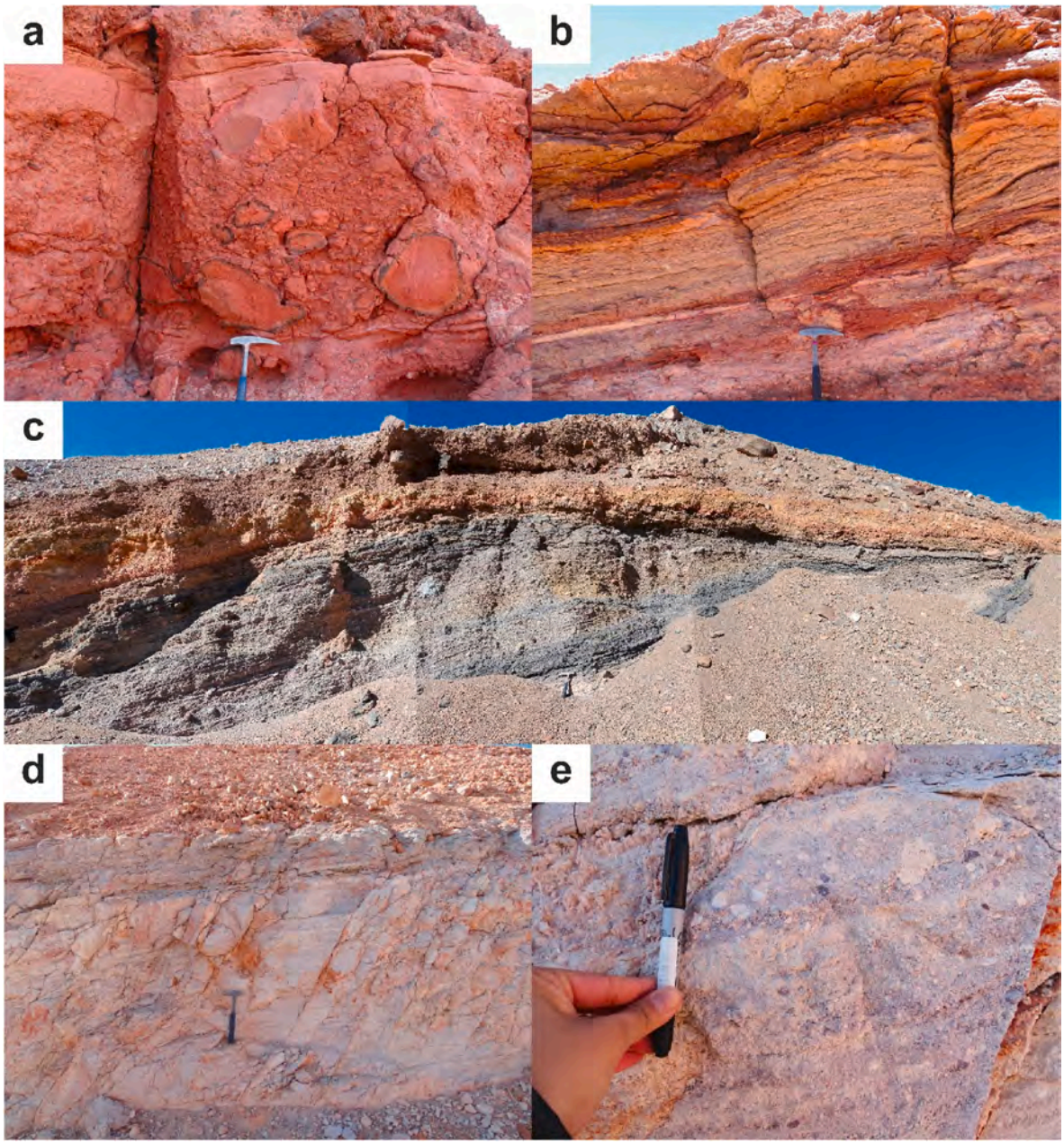


Fig. 12. Folded Middle Miocene volcanoclastic sequence (Salares Norte and Aster 2 sequences).
a) Tilted basaltic andesite pyroclastic breccia with large scoria bombs in massive layer with interbedded laminated scoria-rich ash tuffs. b) Folded alluvial and fluvial sandstones and conglomerates interbedded within basaltic andesite lavas. c) Laharic and alluvial deposits with progressive unconformities of the Salares Norte sequence, interbedded with basaltic lavas (not shown in photograph). d) Folded pyroclastic-epiclastic well-stratified sequence. e) Detail of pumice-rich fine lapilli tuffs interbedded with coarse grained epiclastic pumice-rich sandstones.

and block-and-ash pyroclastic breccias of dacitic to rhyolitic compositions, with an estimated maximum thickness of ca. 150 m. The products of this complex are interdigitated with the explosive and intrusive facies of a synchronous phreatomagmatic volcanism (part of the volcanic complex), associated with a small but profuse maar field, where the occurrence of at least 20 maar-diatreme systems has been identified, many of them with elliptical paleocrater morphologies oriented along a NNE-SSW axis. These explosive structures are intimately related spatially and temporally to areas affected by intense HS-type hydrothermal alteration. The maars, in turn, form a strip at least 4 km long oriented NW-SE, associated with a series of sinistral-normal faults, belonging to the Salares Norte basin. The rocks of the Brecha Principal Volcanic Complex are affected by sinistral strike-slip faults reactivated as normal NW-SE-trending faults, as well as dextral strike-slip faults of NE-SW orientation. These faults are characterized by having little displacement, although they are strongly correlated with the occurrence of pervasive hydrothermal alteration. On the other hand, the emplacement of the domes is often controlled by conduits previously used by the phreatomagmatic feeder dikes, which is why most of them are located on the edge of phreatomagmatic conduits. The phreatomagmatic rocks include pyroclastic rocks as well as a series of subvolcanic dikes and plugs emplaced synchronously to a late-stage in relation to the phreatomagmatic explosions.

Within the phreatomagmatic rocks, the following facies are recognized, using the original definition of Lorenz (2003) modified by Droguett et al. (2019): tuff breccias to pyroclastic breccias, with up to 1 m in diameter lithic fragments and abundant laminated ash tuffs and lapilli tuffs intra-clasts, related to diatreme conduit facies and upper conduit

facies of a maar; stratified to laminated fine lapilli tuffs to fine-grained ash tuffs with gray silicified fragments altered by opaline silica and pumice fragments replaced by jarosite and alunite, including blocks up to 1 m in diameter with puzzle-like fracturing, related to the upper conduit facies of the maar; ash tuffs to fine lapilli tuffs, lithic and/or pumice-rich, (Fig. 13a), with undulated dense juvenile glassy fragments (Fig. 13b), associated with in the internal border facies; and finally, finely laminated fine ash tuffs to fine lapilli tuffs, with subhorizontal disposition (Fig. 13c), characterized by bomb sag structures, associated with the subaerial tuff ring facies of the maar. The tuffs show very variable stratification, strikes and dips ranging from subhorizontal to 75° (Fig. 13d).

A series of dikes and subvolcanic dikes, mainly dacitic in composition, moderately to strongly affected by hydrothermal alteration are common within the phreatomagmatic centers. They intrude the phreatomagmatic tuffs showing undulated borders and, locally, are disaggregated within the tuffs showing undulated and irregular contacts, suggesting a late-stage emplacement within the maar formation cycle when the pyroclastic deposits filling the vent were still hot and probably partly fluidized (Fig. 13e and f).

Following this last phreatomagmatic event known until today, the area was the site of predominantly effusive and, to a lesser extent,

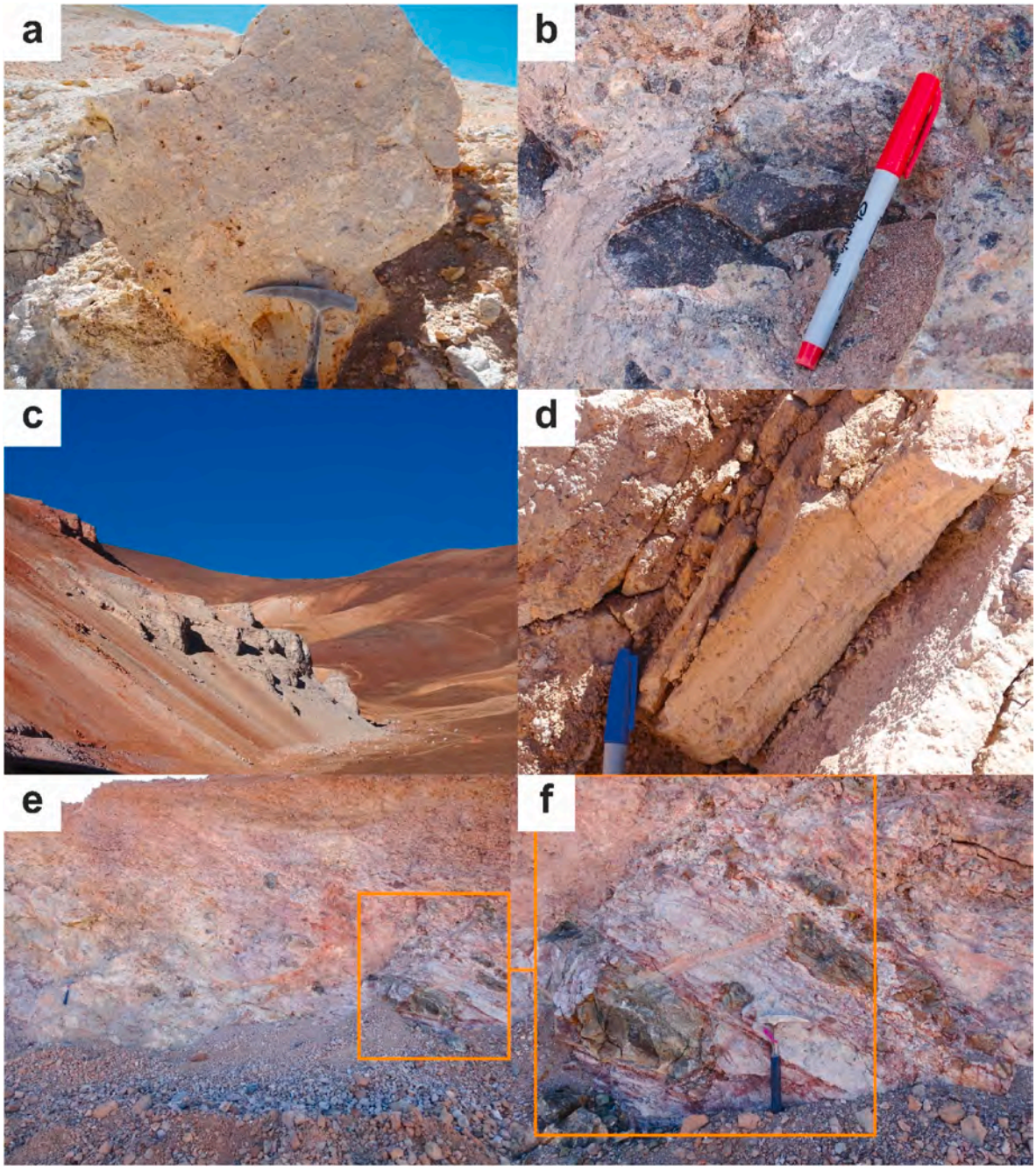


Fig. 13. Examples of phreatomagmatic and subvolcanic rocks associated to maar structures in the southern segment of the Salares Norte belt.
a) Pumice-rich inclined medium lapilli tuff. b) Detail of a dense and glassy juvenile fragment with irregular and undulated borders within a fine-to-medium lapilli pumice-lithic tuff. c) Subhorizontal intra-crater phreatomagmatic sequence up to 60 m thick. d) Detail of steeply dipping ash and fine lapilli phreatomagmatic tuffs. e) Mainly massive phreatomagmatic breccias and coarse lapilli tuffs intruded by dacitic dike. f) Detail of disaggregated intra-maar dike mixed with phreatomagmatic tuffs.

proximal explosive volcanism, essentially andesitic-silicic to dacitic in composition (Upper Miocene-Pliocene; Clavero et al., 1998; Naranjo et al., 2013a,b). Finally, in the Middle Pleistocene (Naranjo and Cornejo, 1992), a small explosion caldera and a posthumous dome formed in the central-eastern part of the segment, known as the Chato Aislado Volcanic Complex. Fig. 14 shows a regional view of the main part of the Salares Norte District and the main volcanic and volcanoclastic units that crop out in the area.

4.2.3.5. Phreatomagmatic volcanism. In this southern segment of the volcanic belt, maar fields or clusters have been identified in at least four areas, although other areas also present phreatomagmatic rocks that could be associated to this type of explosive vents.

The oldest phreatomagmatic volcanism identified in this segment (approximately 15-14 Ma) is exposed in a restricted area in the NW sector, where at least 5 maar-diatreme structures have been identified. Since these structures are faulted and the outcrops lack continuity, it has not been possible to infer the orientation or size of the paleocraters that make up the maar field.

The next phreatomagmatic event occurred around 12–13 Ma and was concentrated in the southwestern sector of the segment. In this area, a maar field consisting of at least ten maar-diatreme systems has been identified, concentrated in a strip up to 4 km in length oriented in the NNW-SSE direction. It has been inferred that the crater diameters on the paleosurface where they formed ranged from approximately 250 to 1000 m, with depths reaching up to 700 m. Some of the structures are affected by sinistral normal faults with a WNW-ESE orientation and by dextral normal faults with a NE-SW orientation, in addition to a series of minor sinistral strike-slip faults NNW-SSE orientated. In the Tres Puntas volcano, the southernmost part of this area, the rocks of this unit are located in the central part of a volcanic complex, where at least five phreatomagmatic centers have been recognized, most of which are aligned in a NW-SE orientation. While no structure affecting the rocks of this unit has been identified so far, a NW-SE trending lineament parallel to regional sinistral strike-slip faults located both to the north and south of the phreatomagmatic centers can be observed.

Finally, the products of the youngest (so far) recognized phreatomagmatic explosive event in this segment of the Salares Norte Belt (ca. 8–9 Ma) essentially crops out in the central sector within the Brecha Principal Volcanic Complex and extend to the surrounding sectors. To date, more than twenty maar-diatreme structures have been identified in the sector (Fig. 15), which exhibit varying degrees of erosion and preservation. Despite this, according to the phreatomagmatic facies recognized (Lorenz, 2003; Ross et al., 2017; Droguett et al., 2019) it is possible to infer and project crater diameters on the paleosurface where they formed, ranging from approximately 500 to 1500 m, with estimated depths of up to 1000 m. This maar field is oriented primarily in the NW-SE direction, parallel to the main faults associated with the Salares Norte basin, although locally many of the centers are elongated in the NE-SW direction (Fig. 15). Most of the maars are also spatially, genetically, and temporally associated with several dacitic dikes and plugs, partly affected by hydrothermal alteration. The phreatomagmatic rocks are cut by sinistral strike-slip faults reactivated as normal faults with an NW-SE direction, as well as a series of dextral strike-slip faults with a NE-SW direction (Fig. 15). These faults are characterized by having limited displacement; however, they often have a strong correlation with the occurrence of sectors affected by pervasive hydrothermal alteration.

4.2.3.6. Age and hydrothermal alteration. The maar fields identified in this segment of the belt are partially to almost completely affected by various types and degrees of HS epithermal alteration. The phreatomagmatic tuffs show evidence of multiple explosive events, partly contemporaneous with the circulation of active hydrothermal fluids. The alteration mineral relationhips indicate the occurrence of at least 3 to 5 discrete and different hydrothermal alteration events that affected the rocks, especially in the Brecha Principal Volcanic Complex area. The fluid circulation associated to these hydrothermal events was concentrated primarily in the phreatomagmatic rocks and in the most permeable levels of the surrounding country rock adjacent to the explosive structures, such as block and ash flow type pyroclastic breccias, epiclastic layers and/or autoclastic parts of lavas of diverse compositions. However, the fluid circulation benefited largely of the tectonic fracturing associated to the synchronic phases of basin formation and later rearrangements, which also helped to generate magma suction and feed the volcanic structures (maars, domes, intrusions).

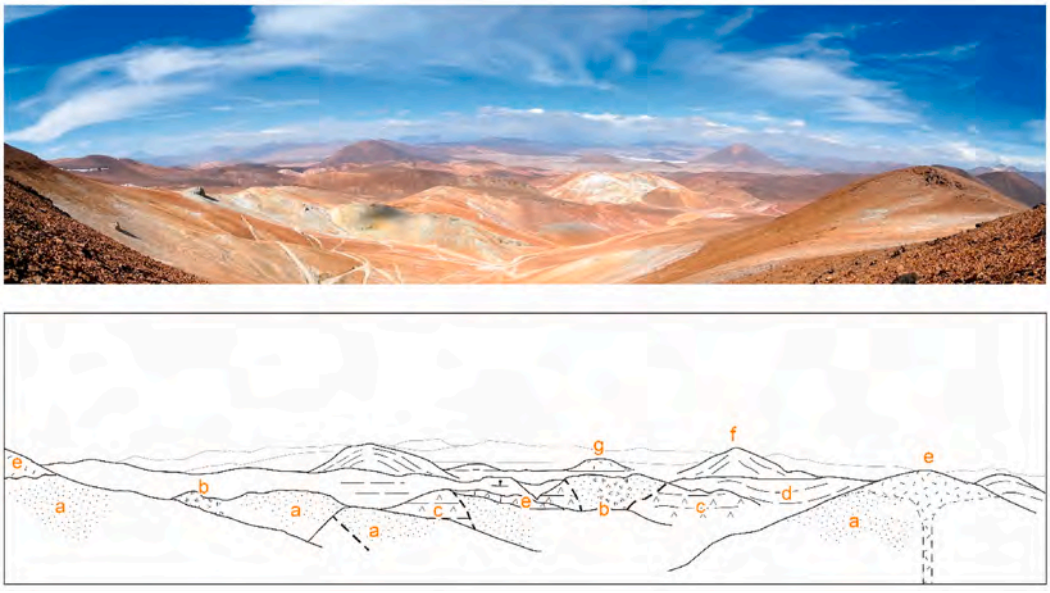


Fig. 14. Regional perspective of the Salares Norte District (view towards the East).
a) Hydrothermally altered phreatomagmatic tuffs, massive to well-stratified; b) Hydrothermally altered phreatomagmatic breccias; c) Upper Miocene rhyodacitic to rhyolitic Brecha Principal dome complex d) Folded Middle Miocene Salares Norte volcanoclastic sequence; e) Post-phreatomagmatic lavas and domes; f) Salar Grande volcano (Upper Miocene); g) Chato Aislado dome and explosive caldera (Pleistocene).

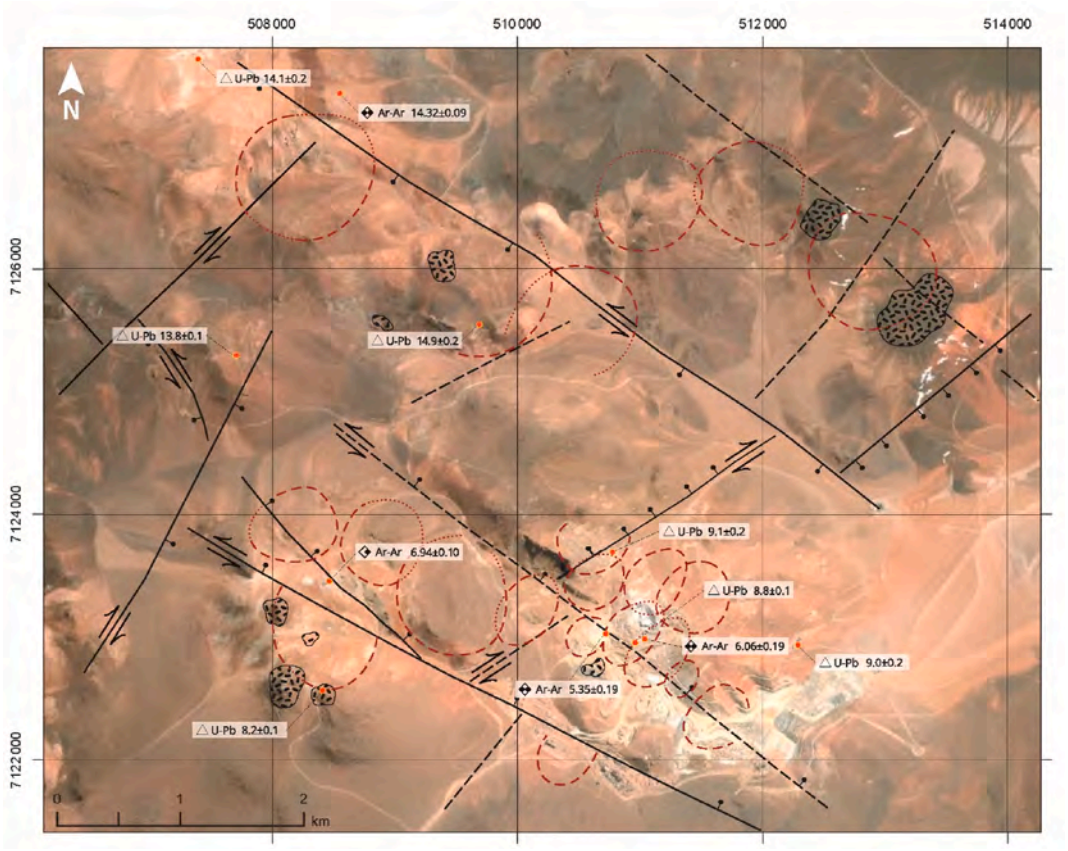


Fig. 15. Structural and volcanological framework of the Salares Norte epithermal District area.
Detail figure (square in Fig. 11) showing the inferred phreatomagmatic paleocraters in dashed red lines and post-alteration exogenous domes as filled black polygons are shown.

In this southern segment of the belt, which partially coincides with the well-known Salares Norte District, the occurrence of at least 5 hydrothermal alteration events affecting the rocks of the area has been determined. These events are estimated to have occurred at approximately 14 Ma, 12 Ma, ca. 8-7 Ma, ca.6.5 Ma, and ca. 5.6 Ma. Based on the available ages of both the phreatomagmatic rocks and alteration in this segment, it is possible to infer that the three explosive phreatomagmatic events represented in this area were accompanied by synchronous and closely linked hydrothermal alteration events that were generated by the same magmatism responsible for both processes (phreatomagmatic explosions and hydrothermal alteration). While no subvolcanic magma bodies have yet been identified associated with the two youngest hydrothermal alteration events, it cannot be ruled out that they may also be related to discrete superimposed phreatomagmatic volcanism in the same area. However, this is still challenging to determine due to the complexity of these structures and the intense alteration affecting the rocks.

5. Discussions

The epithermal exploration prospects located in the area newly named in this work as the Salares Norte Belt have so far been considered, at least informally, as part of the northern segment of the Maricunga Belt. However, both their geographical location and their geological, tectonic, volcanic, and geochronological characteristics allow for a clear differentiation between the epithermal systems in this sector and those found in the well-known Maricunga Belt.

5.1. Tectonics and regional geology

From a tectonic and regional geological perspective, the axis of the Salares Norte Belt is situated about 35–40 km to the east of the main axis of the Maricunga Belt. The western boundary of the epithermal systems in the former is located about 5–10 km to the east of the easternmost systems recognized as part of the Maricunga Belt (Sillitoe et al., 1991; Kay et al., 1999). This more eastern location reflects that the epithermal systems of the Salares Norte Belt are associated with generally younger magmatism than those of the Maricunga Belt, which, in turn, is linked to the migration of the magmatic arc in the Late Cenozoic in this region of the Puna (e.g. Kay et al., 1994; Mpodozis et al., 1995). This younger age of volcanism is likely one of the causes that delayed the exploration of epithermal systems in this area for several decades (Azevedo et al., 2015).

On the other hand, the basement of the epithermal and porphyry-type systems in the Maricunga Belt is primarily composed of Paleozoic, Mesozoic, and Lower Cenozoic rocks, heavily deformed and faulted, associated with deformation systems primarily oriented NS (Mpodozis et al., 2012, 2018). Over these rocks, dome complexes and associated pyroclastic facies have formed (Davidson and Mpodozis, 1991; Mpodozis et al., 1995, 2018), along with a series of subvolcanic intrusions of hypabyssal emplacement in porphyry-type systems (e.g. Muntean and Einaudi, 2000, 2001; Sillitoe et al., 2013). Occasionally, occurrences of phreatomagmatic and phreatic breccias have been locally described (e.g. Gamonal, 2015; Lohmeier et al., 2019), though they constitute minority facies compared to the intrusive.

In contrast, the older units in which the magmatism giving rise to the epithermal systems of the Salares Norte Belt has developed, correspond to gently folded Upper Oligocene to Middle Miocene volcanic and

volcanoclastic sequences, such as the Río Juncalito and Sierra de Aliste Strata (23–26 Ma and 18–20 Ma; Clavero et al., 1998), as well as a series of local volcanoclastic sequences from the Lower and Middle Miocene recognized in this study. Limited remnants of older units (Permian--Triassic granitoids and volcanic rocks; Clavero et al., 1998, 2012) are found on the western to southwestern edge of the belt, associated with compressive NS-oriented structures with their main activity occurring in the Lower Miocene (Mpodozis and Clavero, 2002). These older units likely did not play a significant role in the formation of the Salares Norte epithermal systems, nor in the emplacement of maar fields or the circulation of hydrothermal fluids. The epithermal systems associated with the maar fields of the Salares Norte Belt have thus been emplaced in gently folded, younger volcanoclastic sequences than those of the Maricunga Belt, primarily linked to magmatism controlled by transpressive and transtensive systems that generated the maar fields in the Middle and Upper Miocene, as identified in this study.

5.2. Structures, basins and permeability

The local stress field calculated in the Salares Norte Belt area are compatible with the deformation described by Hoffmann-Rothe et al. (2006) since 16 Ma to the present. In this period the NS-striking Precordilleran Fault System records dextral displacements, which is compatible with sinistral NW-striking, dextral NE-striking fault systems, and ENE-striking extensional fractures (Fig. 16). This fault system may act as conduit of hydrothermal mineralized fluids, which can migrate and precipitate in permeable zones like a favorable lithology, or a fractured open space (e.g. Hedenquist et al., 2000; Rhys et al., 2021; Richards and Tosdal, 2001), which in the case of the Salares Norte Belt usually correspond both to the phreatomagmatic rocks within maar-diatrema systems and permeable layers within the country rock of the phreatomagmatic explosions. Under the stress field calculated it is possible to understand the dynamic interaction between the fault systems, thus, to interpret the increased permeability zones and their geometry (Fig. 16a). The ENE-striking σ1 and NNW-striking σ3, allows to open NE-to EW-striking fractures, which are favorable to build intra-arc basins enable to host both volcanoclastic small basins and volcanic vents, including maar-diatreme systems (Fig. 16b). The transtensional basin together with specific structural geometries like dilatational jogs, pull apart basins, horse tails and some fault intersection, create the condition where the local stress field flip the stress axis σ_1 with σ_2 in these particular geometries. This local extensional stress field favors the fluid circulation and phreatic water accumulation, that is a perfect setting for both for generating repetitive phreatomagmatic activity and hydrothermal fluid circulation.

5.3. Volcanics

From a volcanic-magmatic perspective, we have identified in this southern sector of the Puna, the existence of periods of intense and abundant phreatomagmatic volcanism in the Upper Cenozoic, particularly between the Middle Miocene and Upper Miocene (approximately 15-6 Ma). These periods were previously not recognized at a regional scale in this area (Clavero et al., 2012; Naranjo et al., 2013b, 2016). This volcanism has produced discrete maar-diatreme structures (e.g., Lorenz, 2003; Lorenz and Kurszlaukis, 2006; Valentine and White, 2012) near some stratovolcanoes, as well as a series of structurally controlled maar fields associated to transtensive and transpressive systems, synchronous with the formation of small volcano-sedimentary basins. The epithermal systems located in the Salares Norte Belt are characterized by being spatially and temporally associated with these maar fields (Fig. 15). The magmatic events that formed these maar fields were accompanied by the emplacement of abundant shallow subvolcanic bodies of silicic andesite to dacitic composition and exogenous domes of the same compositions. The feeders of domes and subvolcanics utilized both the zones of weakness generated by active tectonics and the weakness zones of the maar-diatreme systems, essentially their rims and conduits. The occurrence of these types of subvolcanic and exogenous bodies is very common in maar fields, where maar-diatreme systems usually contribute only 5–10% of the volcanic structures (Graettinger, 2018).

The two older periods of phreatomagmatic volcanism (Middle Miocene, approximately 14–15 Ma, and around 12–13 Ma) occurred partially synchronously with the formation and infilling of small volcano-sedimentary tectonic basins, as well as with abundant effusive and explosive volcanic activity. The volcanic products range from basaltic andesites to dacites, similar to what occurred in the same area to the west during the Upper Oligocene to Lower Miocene (Clavero et al., 2012; Mpodozis and Clavero, 2002). On the other hand, the two younger periods of phreatomagmatic volcanism (approximately 8–9 Ma and 5–6 Ma) occurred synchronously with the formation of low-volume dome complexes with associated pyroclastic facies, dacitic to rhyolitic in composition.

Within the maar-diatreme systems identified in the Salares Norte Belt, the following phreatomagmatic facies have been recognized, using the original definition by Lorenz (2003), followed by other authors (e.g. Valentine and White, 2012; Ross et al., 2017) and more recently modified by Droguett et al. (2019): i) main conduit or unstratified diatreme facies mainly represented by massive lithic and lithic-pumice breccias;

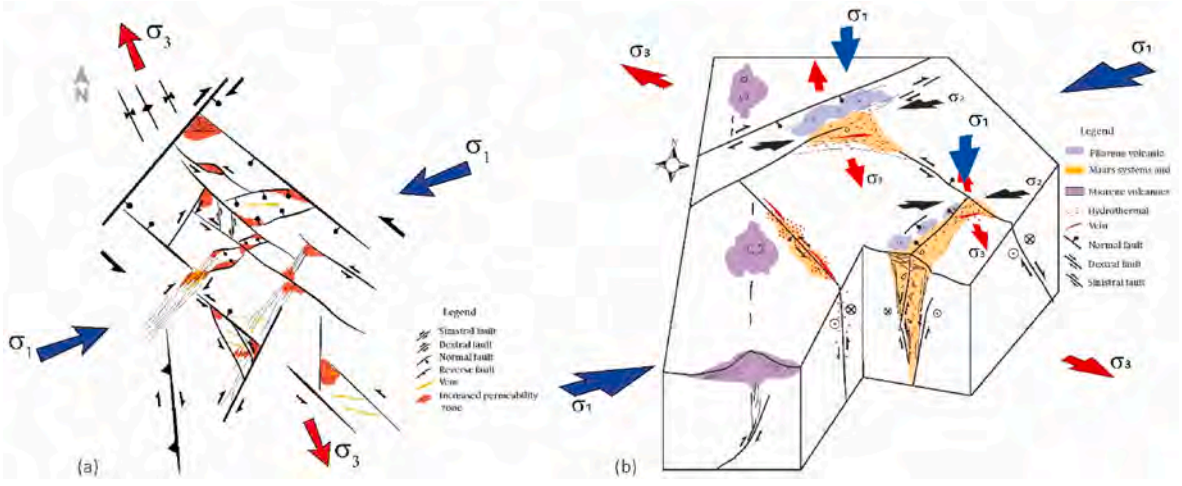


Fig. 16. Structural conceptual model. Relationship between structures, volcanism and hydrothermal fluids
(a) Plan view of structural conceptual model showing the dynamic interaction between principal structural systems. (b) block diagram showing the connection between the principal structural systems and magmatic/hydrothermal fluid channels.

ii) upper conduit facies represented by stratified to laminated fine lapilli tuffs and ash tuffs with lithic megablocks and pyroclastic intra-clasts; iii) medium to deep conduit border facies represented mainly by massive to stratified ash and/or fine lapilli tuffs, pumice and/or lithic-rich, with variable dips between 45° and 75°; iv) upper to middle conduit border facies represented by ash tuffs to fine lapilli tuffs, lithic and/or pumice-rich, massive to stratified with variable stratification and dips ranging from 25° to 50°; and v) subaerial tuff ring maar facies represented by well-stratified/laminated ash tuffs and fine lapilli pumice and/or lithic -rich tuffs, with subhorizontal bedding (mainly parallel and some low-angle cross bedding), commonly showing bomb sag structures. According to the pyroclastic rocks, structures and phreatomagmatic facies identified in these explosive vents and discussed above, mainly associated to the stratified internal maar, the non-stratified conduit and to a lesser extent to the tuff ring facies, it has been possible to infer the projected crater diameters on the paleosurface where they formed, today partially eroded, which vary between 700 and 1500 m, and also that the estimated depths at which the root zone areas are located (Lorenz, 2003) may vary from 600 to over 1000 m.

The composition of the magmas responsible for the phreatomagmatic explosions in these four identified periods was primarily dacitic to rhyolitic, although subvolcanic bodies of silicic andesite composition have also been identified, emplaced at the rims or centers of some maar-diatreme systems. Maar-diatreme systems and maar fields of this composition are a minority compared to those associated with basic magmas worldwide in all types of environments (Graettinger, 2018). As a result, their characteristics have been little described so far, especially their internal structures, which have been proposed to resemble those produced by basaltic-to-basaltic andesite explosions (Ross et al., 2017). This felsic magma composition was also accompanied by processes of high-sulfidation hydrothermal alteration, like other Cenozoic high-sulfidation systems in the Andes located in the Maricunga and El Indio belts, as well as in other sectors of the Andes (e.g., Bissig et al., 2015).

Although it has been suggested that Au–Ag epithermal systems in the Andes are associated with alteration events with scarce synchronous volcanic extrusive phases (Bissig et al., 2015), the direct field relationships, as well as the ages of volcanism and alteration events in the Salares Norte Belt, suggest that alteration events and likely mineralization events have been synchronous with abundant phreatomagmatic and extrusive (effusive and explosive) volcanic events. In addition, subvolcanic phases are ubiquitous but not abundantly recognized in all hydrothermally altered areas of the belt. Moreover, the spatial relationship between hydrothermally altered zones of high-sulfidation type in the Salares Norte Belt and the maar fields, the temporal proximity between explosive volcanic events and hydrothermal alteration events, as well as the presence of fragments with various types of high-sulfidation hydrothermal alteration in the phreatomagmatic breccias and tuffs, suggest that these processes were, in multiple periods, in close spatial-temporal relation, acting repetitively and cyclically.

5.4. Age and hydrothermal alteration

Although there is no geochronological data available for all the phreatomagmatic fields identified so far in the belt, the available data (Tables 1 and 2) indicate the existence of at least 4 discrete events of maar formation in the belt, occurring around 14–15 Ma, 12–13 Ma, 8–9 Ma, and 5–6 Ma. These maar fields are spatially associated with volcanoclastic basins of the Middle Miocene and/or Upper Miocene dome complexes, as can be observed in Figs. 5, Figs. 8 and 11. There is also a direct temporal relationship, in addition to the spatial one, as observed in Figs. 4 and 15, between hydrothermal alteration events and periods of phreatomagmatic volcanism (Tables 1 and 2), suggesting that the magmatic events that formed the maar fields were intimately linked to the origin of the hydrothermal fluids responsible for the HS-type alteration in these systems within the belt.

In some more specific and better-known sectors, such as the Salares Norte District, the occurrence of several of these phreatomagmatic events has been determined, superimposed, and controlled by local transpressive tectonic structures. Fig. 15 shows the inferred phreatomagmatic structures in the central part of the Salares Norte District, an area of the same name that is currently undergoing mine construction. Clusters of maar-diatreme systems are observed, structurally controlled, superimposed, and with complex cross-cutting relationships, as well as a series of post-alteration exogenous domes located both on the edges and near the conduits. These intimate relationships between maar-diatreme systems, structures and hydrothermal alteration, suggest that both primary (pyroclastic) and secondary (tectonic) permeability locally facilitated fluid circulation within these volcanic structures and their immediate surroundings. Moreover, the superposition of maar-diatreme systems and their relationship to tectonic structures suggests that the feeding dikes have continued to utilize the same structures that had formed at the time of the generation of the Middle Miocene volcano-sedimentary basins, in a repetitive manner. The occurrence of

Table 2
Selected geochronological data from Salares Norte District area, shown in Fig. 15.

Sample Code	Unit	UTM East	UTM North	Lithology	Method	Mineral	Age ± 2σ error	Reference
AG-101	Phreatomagmatic volcanism	509675	7125547	Phreatomagmatic medium-to-coarse lapilli tuff	U–Pb	Zircon	14.9 ± 0.2	GoldFields Salares Norte SpA, 2020
FERS-001	Phreatomagmatic volcanism	507373	7127718	Phreatomagmatic lapilli tuff	U–Pb	Zircon	14.1 ± 0.2	This study
AG-258	Phreatomagmatic volcanism	510766	7123684	Phreatomagmatic lapilli tuff	U–Pb	Zircon	9.1 ± 0.2	GoldFields Salares Norte SpA, 2020
AG-09	Phreatomagmatic volcanism	510951	7122943	Phreatomagmatic fine-lapilli tuff	U–Pb	Zircon	8.8 ± 0.1	GoldFields Salares Norte SpA, 2020
AG-23	Upper Miocene volcanic complex	512285	7122924	Block and ash pyroclastic breccia	U–Pb	Zircon	9.0 ± 0.2	GoldFields Salares Norte SpA, 2020
AG-87	Upper Miocene volcanic complex	508392	7122552	Dacite dome	U–Pb	Zircon	8.2 ± 0.1	GoldFields Salares Norte SpA, 2020
A3DD-034	Middle Miocene volcaniclastic sequence	507685	7125296	Altered andesite lava	U–Pb	Zircon	13.8 ± 0.1	This study
A3DD026	Hydrothermal alteration	508533	7127437	Altered andesite lava	Ar–Ar	Natroalunite	14.32 ± 0.09	GoldFields Salares Norte SpA, 2020
AG-292	Hydrothermal alteration	508446	7123448	Altered phreatomagmatic tuff	Ar–Ar	Jarosite	6.94 ± 0.10	GoldFields Salares Norte SpA, 2020
SN-DAT-08	Hydrothermal alteration	511029	7122973	Altered phreatomagmatic tuff	Ar–Ar	Alunite	6.06 ± 0.19	Santos (2014)
SN-DAT-05	Hydrothermal alteration	510711	7123016	Altered phreatomagmatic tuff	Ar–Ar	Alunite	5.35 ± 0.19	Santos (2014)

synchronic explosive phreatomagmatic vents with effusive domes suggests that the transition from explosive phases to effusive volcanic phases probably depended on the specific occurrence, localization, and volume of phreatic water tables. In Fig. 15, the direct relationships between the phreatomagmatic structures, the tectonic structures and the areas affected by HS hydrothermal alteration can be observed, while in Tables 2 and it can be established that at least two hydrothermal alteration events (^{40}Ar-^{39}Ar ages in alunite or jarosite around 14.3 Ma and ca. 8.8 Ma) are synchronous, within the errors of the geochronological methods, with the formation of phreatomagmatic tuffs and breccias in this specific part of the belt.

It is interesting to note that the ages of the two oldest phreatomagmatic-volcanic events coincide with the ages of the younger volcanic events associated with alteration/mineralization in the Maricunga Belt (e.g. Casale, Chen et al., 2010; Cáceres, 2015; Cerro Maricunga, Lohmeier et al., 2019; La Coipa, Gamonal et al., 2015). Meanwhile, the younger events have age similarities with other more distant epithermal systems in the Andes of Chile. For example, the 8–9 Ma event partially overlaps with the epithermal system of Choquelimpie in the Arica Altiplano (Gröpper et al., 1991; Ordóñez and Rivera, 2004) where phreatomagmatic facies have also been described (Clavero et al., 2018), while the youngest event partly overlaps with the younger alteration and associated volcanic phases of the El Indio Belt (Martin et al., 1995; Clavero et al., 1997; Jannas et al., 1999; Bissig et al., 2015), as well as the earliest part of the volcanic activity associated with the epithermal system of Anocarire in the Altiplano of Arica (Droguett et al., 2023).

6. Conclusions

The epithermal Au–Ag Salares Norte belt is located about 35 km east of the axis of the Oligo-Miocene metallogenic Maricunga belt. The high-sulfidation (HS) epithermal systems found within the Salares Norte Belt are spatially and temporally associated with maar fields formed by various discrete events of abundant phreatomagmatic volcanism that occurred during the Middle to Upper Miocene. The emplacement of these maar fields was structurally controlled by systems essentially oblique to the main arc, oriented NE-SW, and NW-SE, which in turn generated small basins filled with volcano-sedimentary and volcanic materials. Some of these volcanoclastic and volcanic sequences served as country rock of the phreatomagmatic explosions. The oldest units in which the basins formed, and the maar fields were emplaced correspond to Upper Oligocene-Lower Miocene volcanoclastic sequences, mainly towards the western edge of the belt.

Local transpressive to transtensive tectonics allowed for the repetitive ascent of magmatic dikes, which encountered water tables at very shallow crustal levels within the volcanoclastic filling of these basins. This resulted in the formation of maar fields with complex morphologies, featuring abundant nested or cross-cutting maar-diatreme systems. These maar fields were accompanied by abundant shallow subvolcanic intrusive bodies and exogenous domes, with their feeder dikes using both tectonic structures and the weakness zones of the volcanic structures (maar rims and conduits) for their emplacement.

Hydrothermal alteration events, synchronous with at least 3 out of the 4 phreatomagmatic volcanic events, utilized not only the high primary permeability provided by phreatomagmatic fragmental rocks but also the shear zones and intense fracturing associated with local tectonics, as well as more permeable levels within the country rock where the maars developed.

In summary, the epithermal systems of the Salares Norte Au–Ag Belt have formed in a geological, tectonic, and volcanic environment that is distinct from that of the Maricunga Belt. This distinction allows it to be separated as a younger metallogenic belt with well-defined geological, volcanological, and structural characteristics.

CRediT authorship contribution statement

J. Clavero: Writing – review & editing, Writing – original draft, Visualization, Validation, Supervision, Project administration, Investigation, Funding acquisition, Formal analysis, Conceptualization. **P. Pérez-Flores:** Writing – review & editing, Writing – original draft, Validation, Investigation, Formal analysis, Data curation, Conceptualization. **F. Rojas:** Visualization, Project administration, Funding acquisition, Conceptualization. **D. Huete-Verdugo:** Visualization, Project administration, Funding acquisition, Conceptualization. **B. Droguett:** Writing – original draft, Investigation, Formal analysis, Data curation. **V. Ramírez:** Methodology, Investigation, Formal analysis, Data curation.

Declaration of competing interest

The authors declare that they have no known competing financial interests or personal relationships that could have appeared to influence the work reported in this paper.

Data availability

The authors do not have permission to share data.

Acknowledgements

The authors acknowledge the financial and logistical support, as well as the publication authorization granted by Gold Fields Salares Norte SpA. The manuscript was certainly improved by the comments done by Dr. A. Folguera and an anonymous reviewer. The authors also extend their gratitude to the exploration geologists A. Cancino, N. Rojas, A. Acevedo, C. Seguel, C. Cerda, T. Guevara, and J. Rodríguez, for their valuable conversations and discussions about the geology, geochronology, and structures of the Salares Norte District. The work benefited from the valuable collaboration of G. Anabalón and A. Sancho in figure production, and of J. Lemp, A. Sancho, J. Ramírez, V. Reyes, and R. Reyes in the field work.

References

Angelier, J., 1984. Tectonic analysis of fault slip data sets. J. Geophys. Res. 89, 5835–5848.

Araneda, R., 1982. El Indio, yacimiento de oro, plata y cobre, Coquimbo, Chile. Minerales 37 (160), 5–13.

Azevedo, F., Brewer, N., Santos, A., Huete Verdugo, D., Baumgartner, R., Roncal, L., Trueman, A., Foley, A., 2015. The discovery and geology of the Salares Norte epithermal gold-silver deposit, northern Chile. In: NewGenGold Conference, Perth, Australia.

Beck, M.E., 1991. Coastwise transport reconsidered: lateral displacements in oblique subduction zones, and tectonic consequences. Phys. Earth Planet. In. 68, 1–8. https://doi.org/10.1016/0031-9201(91)90002-Y.

Bissig, T., Lee, J.K.W., Clark, A.H., Heather, K.B., 2001. The Cenozoic history of volcanism and hydrothermal alteration in the Central Andean flat-slab region: new ^{40}Ar-^{39}Ar constraints from the El Indio-Pascua Au (-Ag, Cu) belt, 29°20' - 30° 30'S. Int. Geol. Rev. 43, 312–340.

Bissig, T., Clark, A., Rainbow, A., Montgomery, A., 2015. Physiographic and tectonic settings of high-sulfidation epithermal gold–silver deposits of the Andes and their controls on mineralizing processes. Ore Geol. Rev. 65, 327–364.

Blanquat, M.D. Saint, Tikoff, B., Teyssier, C., Vigneresse, J.L., 1998. Transpressional kinematics and magmatic arcs. Geol. Soc. , London , Spec. Publ. 135, 327–340. https://doi.org/10.1144/GSL.SP.1998.135.01.21.

Cáceres, M., 2015. Nuevos antecedentes geocronológicos del Distrito Casale, sur de la Franja Maricunga, Región de Atacama, Chile. In: Congreso Geológico Chileno, vol. 2. Actas, La Serena, pp. 44–47. No 14.

Chang, Z., Vervoort, J.D., McClelland, W.C., Knaack, C., 2006. U-Pb dating of zircon by LA-ICP-MS. G-cubed 7 D (5), Q05009. https://doi.org/10.1029/2005GC001100. Washington.

Chen, H., Hollings, P., Cooke, D., Gemmell, B., 2010. Lithocap and porphyritic alteration and mineralization in the Cerro Casale district, Chile: implications for exploration. In: AMIRA P765A - Geochemical and Geological Halos in Green Rocks and Lithocaps: the Explorers' Toolbox for Porphyry and Epithermal Districts, Final Sponsors Meeting, Hobart, vol. 3, pp. 4.1–4.32. December 8th 2010.

Chernicoff, C.J., Richards, J.P., Zappettini, E.O., 2002. Crustal lineament control on magmatism and mineralization in northwestern Argentina: geological, geophysical,

and remote sensing evidence. Ore Geol. Rev. 21, 127–155. https://doi.org/10.1016/S0169-1368(02)00087-2.
Clavero, J., Martin, M., Mpodozis, C., Cuitiño, L., 1997. Eventos de alteración-mineralización en la Franja El Indio. Congreso Geológico Chileno, Antofagasta, Chile.
Clavero, J., Gardeweg, M., Mpodozis, V., 1998. Mapa Geológico preliminar del Área del Salar de Piedra Parada. In: Región de Atacama. Servicio Nacional de Geología y Minería, Santiago. Mapas Geológicos, Versión preliminar, escala1:100.000.
Clavero, J., Mpodozis, C., Gardeweg, M., Valenzuela, M., 2012. Geología de las Áreas Laguna Wheelwright y Paso San Francisco, Región de Atacama, vols. 139–140. Servicio Nacional de Geología y Minería, Carta Geológica de Chile, Serie Geología Básica, Santiago, p. 32, 1 mapa escala 1:100.000.
Clavero, J., Droguett, B., Quiroga, R., Álvarez, P., 2018. Carta lago Chungará, región de Arica y Parinacota. Servicio Nacional de Geología y Minería, Carta Geológica de Chile. Serie Geología Básica 194, 1 mapa escala 1:100.000. Santiago.
Cornejo, P., Mpodozis, C., Ramírez, C.F., Tomlinson, A., 1993. Estudio Geológico de la región de El Salvador y Potrerillos. In: Servicio Nacional de Geología y Minería CODELCO, Informe Registrado, 1. p, Santiago, Chile, p. 250.
Cornejo, P., Mpodozis, C., Rivera, O., Matthews, S., 2009. Carta exploradora, regiones de Antofagasta y atacama. Servicio nacional de Geología y minería. In: Carta Geológica de Chile, Serie Geología Básica, vol. 119, p. 9, 1 mapa escala 1:100.000. Santiago.
Cornejo, P., Mpodozis, C., Tomlinson, A.J., 1998. Hoja salar de Maricunga, región de Atacama. In: Servicio. Nacional de Geología y Minería, Mapas Geológicos No.7, 1 mapa escala 1:100.000. Santiago.
Davidson, J., Mpodozis, C., 1991. Regional geologic setting of epithermal gold deposits, Chile. Econ. Geol. 86 (6), 1174–1186.
Droguett, B., Clavero, J., Quiroga, R., 2019. Facies Analysis of an Eocene to Lower Miocene Phreatomagmatic Volcanic Field in the Andes of Central Chile. IUGG General Assembly, Montreal, Canada.
Droguett, B., Clavero, J., Álvarez, P., Ramírez, V., 2023. Geología de las áreas Surire-Tignamar y Quilhuiri, regiones de Arica y Parinacota y Tarapacá. Servicio Nacional de Geología y Minería, Carta Geológica de Chile, Serie Geología Básica, Santiago, pp. 217–218, 230pp., 1 map scale 1:100.000.
ENAMI, 2018. Prospecto Tres Puntas. In SIGEX (Sistema de Información Geológica de Exploración). Servicio Nacional de Geología y Minería, Chile.
Fossen, H., Tikoff, B., Teyssier, C., 1994. Strain modeling of transpressional and transtensional deformation. Nor. Geol. Tidsskr.
Gardeweg, M, Ramírez, C.F., Davidson, J., 1993. Mapa Geológico del área del Salar de Punta Negra y del volcán Llullaillaco, Región de Antofagasta. Servicio Nacional de Geología y Minería, Documentos de Trabajo, Santiago, Chile. No. 5, escala 1: 100.000.
Galina, M., 2019. Geología y Metalogénesis del depósito epitermal de alta sulfuración El Guanaco, Desierto de Atacama, Chile. Facultad de Ciencias Naturales y Museo Universidad Nacional de La Plata 224. Tesis Doctoral.
Gamonal, S., 2015. Volcanic Stratigraphy and Epithermal Mineralization of the La Coipa District, Maricunga Belt, Chile. University of British Columbia, Canada, p. 306p. MSc thesis.
Gamonal, S., Bissig, T., Fletcher, D., Shroer, G., den Boer, D., Jemielita, R., 2015. Oligocene to Miocene volcanic and hydrothermal history and revised early to middle Miocene Ag-Au mineralization ages of the La Coipa district, Maricunga belt. In: Congreso Geológico Chileno, vol. 2. Actas, La Serena, pp. 44–47, 14.
Gardeweg, M.C., Mpodozis, C., Clavero, J., 1998. The Ojos del Salado Complex: the highest active volcano of the world. In: I.A.V.C.E.I. general Assembly, Cape Town, South Africa. Abstracts on Magmatic Diversity: Volcanoes and their roots, p. 21.
Gardeweg, M.C., Mpodozis, C., Clavero, J., Cuitiño, L., 1997. Mapa Geológico de la Hoja Nevado Ojos del Salado, Región de Atacama. Escala 1:1.00.000. Servicio Nacional de Geología y Minería, Chile.
Giambiagi, L., Álvarez, P.P., Creixell, C., Mardonez, D., Murillo, I., Velásquez, R., Lossada, A., Suriano, J., Mescua, J., Barrionuevo, M., 2017. Cenozoic shift from compression to strike-slip stress regime in the high andes at 30°S, during the shallowing of the slab: implications for the el indio/tambo mineral district. Tectonics 36, 2714–2735. https://doi.org/10.1002/2017TC004608.
Gold Fields Salares Norte SpA, 2020. Internal report by Amawta Geoconsultores "Levantamiento geológico-estructural Distrito Salares Norte, Cordiller Principal de la región de Atacama, Chile". Unpublished internal report, p. 93.
Graettinger, A., 2018. Trends in maar crater size and shape using the global Maar Volcano Location and Shape (MaarVLS) database. J. Volcanol. Geoth. Res. 357, 1–13.
Gröpper, H., Calvo, M., Crespo, H., Bisso, C., Cuadra, W., Dunkerley, P., Aguirre, E., 1991. The epithermal gold-silver deposit of Choquelimpie, Northen Chile. Econ. Geol. 86, 1206–1221.
Grosse, P., Orihashi, Y., Guzmán, S.R., Sumino, H., Nagao, K., 2018. Eruptive history of Incahuasi, falso Azufre and el cóndor quaternary composite volcanoes, southern central andes. Bull. Volcanol. 80 (44) https://doi.org/10.1007/s00445-018-1221-5.
Hedenquist, J.W., Arribas, A., Gonzalez-Urien, E., 2000. Exploration for epithermal gold deposits. SEG Rev 13, 245–277 doi.org/07410123.
Hoffmann-Rothe, A., Kukowski, N., Dresen, G., Echtler, H., Oncken, O., Klotz, J., Scheuber, E., Kellner, A., 2006. Oblique convergence along the Chilean Margin: partitioning, margin-parallel faulting and force interaction at the plate interface. In: Oncken, O., Chong, G., Franz, G., Giese, P., Götze, H.-J., Ramos, V.A., Strecker, M.R., Wigger, P. (Eds.), The Andes: Active Subduction Orogeny. Springer Berlin Heidelberg, Berlin, Heidelberg, pp. 125–146. https://doi.org/10.1007/978-3-540-48684-8_6.
Holley, E.A., Bissig, T., Monecke, T., 2016. The Veladero high-sulfidation epithermal gold deposit, El Indio-Pascua Belt, Argentina: geochronology of alunite and jarosite. Econ. Geol. 111, 311–330. https://doi.org/10.2113/econgeo.111.2.311.
Hu, J., Liu, L., Hermosillo, A., Zhou, Q., 2016. Simulation of late cenozoic South American flat-slab subduction using geodynamic models with data assimilation. Earth Planet Sci. Lett. 438, 1–13. https://doi.org/10.1016/j.epsl.2016.01.011.
Inversiones Barrick Conosur Ltda, 2022. Prospecto Azufreras. In SIGEX (Sistema de Información Geológica de Exploración). Servicio Nacional de Geología y Minería, Chile.
Jannas, R.R., Bowers, T.S., Petersen, U., Beane, R.E., 1999. High-sulfidation deposit types in the el Indio district, Chile. Spec. Publ. Soc. Econ. Geol. 7, 219–266.
Jovic, S., Guido, D., Paez, G., Galina, M., 2015. Marco tectónico y estructural del depósito epitermal de alta sulfuración El Guanaco, Antofagasta, Chile. XIV Congreso Geológico Chileno, La Serena.
Kay, S.M., Mpodozis, C., Tittler, A., Cornejo, P., 1994. Tertiary magmatic evolution of the Maricunga mineral belt in Chile. Int. Geol. Rev. 36, 1079–1112.
Kay, S., Mpodozis, C., Coira, B., 1999. Neogene magmatism, tectonism, and mineral deposits of the central andes (22°S to 33°S latitude). Geology and Ore Deposits of the Central Andes, Society of Economic Geology, Special Publication 7, 27–59.
Kay, S.M., Burns, W.M., Copeland, P., Mancilla, O., 2006. Upper Cretaceous to Holocene magmatism and evidence for transient Miocene shallowing of the Andean subduction zone under the northern Neuquén Basin. Spec. Pap. Geol. Soc. Am. 407, 19–60. https://doi.org/10.1130/2006.2407(02.
Lohmeier, S., Schneider, A., Belyatsky, B., Lehmann, B., 2019. Magmatic evolution of the Cerro Maricunga gold porphyry-epithermal system, Maricunga belt, N-Chile. J. S. Am. Earth Sci. 92, 374–399.
Lorenz, V., 2003. Maar-diatreme volcanoes, their formation, and their setting in hard-rock or soft-rock environment. Geol Lines 15, 72–83.
Lorenz, V., Kurszlaukis, S., 2006. Root zone processes in the phreatomagmatic pipe emplacement model and consequences for the evolution of maar-diatreme volcanoes. J. Volcanol. Geoth. Res. 159, 4–32.
Ludwig, K.R., 2003. User's Manual for Isoplot 3.00: a Geochronological Toolkit for Microsoft Excel (No.4). Berkeley Geochronological Center, p. 75.
Mccaffrey, K.J.W., 1992. Igneous emplacement in a transpressive shear zone. Ox Mountains igneous complex 149, 221–235.
Martin, M., Clavero, J., Mpodozis, C., Cuitiño, L., 1995. Estudio geológico regional de la Franja el Indio, Cordillera de Coquimbo. In: Informe Registrado IR-95-6, vol. 238p. Servicio Nacional de Geología y Minería, 4 mapas escala 1:50.000.
Martinod, J., Husson, L., Roperch, P., Guillaume, B., Espurt, N., 2010. Horizontal subduction zones, convergence velocity and the building of the Andes. Earth Planet Sci. Lett. 299, 299–309. https://doi.org/10.1016/j.epsl.2010.09.010.
Mpodozis, C., Clavero, J., 2002. Tertiary tectonic evolution of the southwestern edge of the Puna plateau: Cordillera Claudio Gay (26°-27°S), northern Chile. In: International Symposium on Andean Geodinamics No. 5, IRD Editions, Proceedings, pp. 445–448. Toulouse, France.
Mpodozis, C., Cornejo, P., Kay, S., Tittler, A., 1995. La Franja de Maricunga: síntesis de la evolución del Frente Volcánico Oligoceno-Mioceno de la zona sur de los Andes Centrales. Rev. Geol. Chile 22 (2), 273–313.
Mpodozis, C., Kay, S.M., 2003. Neogene tectonics, ages and mineralization along the transition zone between the El Indio and Maricunga mineral belts (Argentina and Chile 28°-29° S). In Congreso Geológico Chileno. In: No, 10. Actas, Concepción.
Mpodozis, C., Kay, S.M., Gardeweg, M., Coira, B., Actas, I.I.I., 1996. Geología de la región de Ojos del Salado (Andes Centrales, 27°S): implicancias de la migración hacia el este del frente volcánico Cenozoico Superior. Geolgico Argentino y Explor. Hidrocarburos 539–548. SRC-GoogleScholar FG-0.
Mpodozis, C., Iriarte, S., Gardeweg, M., Valenzuela, M., 2012. Carta Laguna del Negro Francisco, Región de Atacama, vol. 145. Servicio Nacional de Geología y Minería, Carta Geológica de Chile, Santiago, p. 30, 1 mapa escala 1:100.000.
Mpodozis, C., Clavero, J., Quiroga, R., Droguett, B., Arcos, R., 2018. Geología del área Cerro Cadillal-Cerro Jotabeche, región de Atacama. Servicio Nacional de Geología y Minería, Carta Geológica de Chile, Serie Geología Básica 200, 1 mapa escala 1: 100.000.
Muntean, J.L., Einaudi, M.T., 2000. Porphyry gold deposits of the Refugio district, Maricunga belt, northern Chile. Econ. Geol. 95, 1445–1472.
Muntean, J.L., Einaudi, M.T., 2001. Porphyry-epithermal transition: Maricunga belt, northern Chile. Econ. Geol. 96, 743–772.
Naranjo, J.A., 1992. Chemistry and petrological evolution of the Lastarria volcanic complex in the north Chilean Andes. Geol. Mag. 129, 723–740. https://doi.org/10.1017/S0016756800008451.
Naranjo, J., Cornejo, P., 1992. Hoja Salar de La Isla, Región de Antofagasta. Santiago. Servicio Nacional de Geología y Minería, Chile. Carta Geológica de Chile. No 72 escala 1:250.000.
Naranjo, J.A., Ramírez, C., Villa, V., 2016. Geología de las áreas Cerro Panteón de Aliste y Cerro Colorado, Región de Atacama. Servicio Nacional de Geología y Minería, Carta Geológica de Chile, Santiago. Serie Geología Básica 185-186, 1 mapa escala 1: 100.000.
Naranjo, J.A., Villa, V., Venegas, C., 2013a. Geología de las áreas Salar de Pajonales y Cerro Moño, regiones de Antofagasta y Atacama. Servicio Nacional de Geología y Minería, Carta Geológica de Chile, Serie Geología Básica, Nos, Santiago, pp. 153–154, 1 mapa escala 1:100.000.
Naranjo, J., Villa, V., Venegas, C., 2013b. Geología de las Áreas Salar de Aguilar y Portezuelo del León Muerto, Región de Atacama. Servicio Nacional de Geología y Minería, Santiago. Carta Geológica de Chile, Serie Geología Básica: No 151-152, 45 pp. escala 1:100.000.
Naranjo, J.A., Hevia, F., Arcos, R., Polanco, E., 2019a. Geología de las áreas Nevado Ojos del Salado y Cerro El Fraile, Región de Atacama, vols. 204–205. Servicio Nacional de Geología y Minería, Carta Geológica de Chile, Serie Geología Básica, Santiago, p. 96, 1 mapa escala 1:100.000.

Naranjo, J.A., Hevia, F., Villa, V., Ramírez, C.A., 2019b. Miocene to Holocene geological evolution of the Lazufre segment in the Andean volcanic arc. Geosphere 15 (1), 47–59. https://doi.org/10.1130/GES01352.1.

Niemeyer, H., Munizaga, R., 2008. Structural control of the emplacement of the Portrerillos porphyry copper , central Andes of Chile. J. South Am. Earth Sci. 26, 261–270. https://doi.org/10.1016/j.jsames.2008.08.006.

Ordóñez, A., Rivera, G., 2004. Mapa metalogénico de la I región de Tarapacá, Escala 1: 500.000. Servicio Nacional de Geología y Minería.

Otsubo, M., Sato, K., Yamaji, A., 2006. Computerized identification of stress tensors determined from heterogeneous fault-slip data by combining the multiple inverse method and k-means clustering. J. Struct. Geol. 28, 991–997.

Palacios, C., Ramírez, L.E., Townley, B., 2007. The role of the Antofagasta – calama Lineament in ore deposit deformation in the Andes of northern Chile. Miner. Deposita 301–308. https://doi.org/10.1007/s00126-006-0113-3.

Perelló, J., Sillitoe, R.H., Mpodozis, C., Brockway, H., Posso, H., 2012. Geologic setting and evolution of the porphyry copper-molybdenum and copper-gold deposits at los pelambres, Central Chile. Soc. Econ. Geol. Inc. Spec. Publ. 16, 79–104. https://doi.org/10.5382/sp.16.04.

Piquer, J., Skarmeta, J., Cooke, D.R., 2015. Structural evolution of the Rio blanco-los Bronces district , andes of Central Chile : controls on stratigraphy , magmatism and mineralization. Econ. Geol. 110, 1995–2023.

Piquer, J., Yáñez, G., Rivera, O., Cooke, D.R., 2019. Long-lived crustal damage zones associated with fault intersections in the high andes of Central Chile. Andean Geol. 46, 223–239. https://doi.org/10.5027/andgeov46n2-3106.

Rhys, D.A., Lewis, P.D., Rowland, J.V., 2021. Chapter 3: structural controls on ore localization in epithermal gold-silver deposits: a mineral systems approach. Appl. Struct. Geol. Ore-Forming Hydrothermal Syst. 83–145. https://doi.org/10.5382/rev.21.03.

Richards, J.P., Jourdan, F., Creaser, R.A., Maldonado, G., Dufrane, S.A., 2013. Geology, geochemistry, geochronology, and economic potential of Neogene volcanic rocks in the Laguna Pedernal and Salar de Aguas Calientes segments of the Archibarca lineament , northwest Argentina. Journal of Volcanology and Geothermal Research 258, 47–73. https://doi.org/10.1016/j.jvolgeores.2013.04.004.

Richards, J.P., Tosdal, R.M., 2001. Structural Control on Ore Genesis. Society of economic Geology, Inc.

Richards, J.P., Villeneuve, M., 2002. Characteristics of late cenozoic volcanism along the archibarca lineament from Cerro Llullaillaco to Corrida de Cori, northwest Argentina. J. Volcanol. Geoth. Res. 116, 161–200. https://doi.org/10.1016/S0377-0273(01)00329-8.

Ross, P., Carrasco Nuñez, G., Hayman, P., 2017. Felsic maar-diatreme volcanoes: a review. Bull. Volcanol. 79, 20.

Rubiolo, R., Pereyra, L. Martínez y F., 2003. Fiambalá 2769-IV, Provincias de Catamarca y La Rioja, vol. 364. Instituto de Geología y Recursos Minerales, Servicio Geológico Minero Argentino. Boletín N°, Buenos Aires, p. 78.

Santos, A., 2014. Geocronología Salares Norte para Gold Fields Salares Norte SpA. Unpublished internal report.

Seggiaro, R., Becchio, R., Martínez, F. Pereyra y L., 2007. Hoja Geológica 2569-IV, Antofalla, provincias de Catamarca y Salta. Instituto de Geología y Recursos Minerales, vol. 343. Servicio Geológico Minero Argentino, Boletín, Buenos Aires.

Seggiaro, R.E., Hongn, F.D., Castillo, A., Pereyra, F., Martínez, D. Villegas y L., 2006. Hoja Geológica 2769-II, Paso San Francisco, Provincia de Catamarca, vol. 294. Instituto de Geología y Recursos Minerales, Servicio Geológico Minero Argentino. Boletín, Buenos Aires, p. 62.

Sillitoe, R.H., McKee, E.H., Vila, T., 1991. Reconnaissance K-Ar geochronology of the Maricunga gold-silver belt, northern Chile. Econ. Geol. 86, 1261–1270.

Sillitoe, R.H., Tolman, J., van Kerkvoort, G., 2013. Geology of the Caspiche porphyry gold-copper deposit, Maricunga belt, northern Chile. Econ. Geol. 108, 585–604.

Somoza, R., 1998. Updated Nazca (Farallon)-South America relative motions during the last 40 My: implications for mountain building in the central Andean region. J. South Am. Earth Sci. 11, 211–215.

Stern, C.R., Moreno, H., López-Escobar, L., Clavero, J.E., Lara, L.E., Naranjo, J.a., Parada, M.a., Skewes, M.A., 2007. Chilean volcanoes. In: The Geology of Chile. The Geological Society, pp. 147–178.

Teyssier, C., Tikoff, B., Markley, M., 1995. Oblique plate motion and continental tectonics. Geology 23, 447–450. https://doi.org/10.1130/0091-7613(1995)023<0447:OPMACT>2.3.CO;2.

Tomlinson, A., Cornejo, P., Mpodozis, C., 1999. Hoja Potrerillos, Región de Atacama. Servicio Nacional de Geología y Minería, Santiago. Mapas Geológicos No 14, escala1: 100.000.

Valencia, V., Ruiz, J., Barra, F., Geherls, G., Ducea, M., Titley, S., Ochoa-Landín, L., 2005. U-Pb zircon and Re-Os molybdenite geochronology from La Caridad porphyry copper deposit: insight for the duration of magmatism and mineralization in the Nacozari District, Sonora, Mexico. Miner. Deposita 40 (2), 175–191. https://doi.org/10.1007/s00126-0480-1.

Valentine, G., White, J., 2012. Revised conceptual model for maar-diatremes: subsurface processes, energetics, and eruptive products. Geology 40–12, 1111–1114.

Villa, V., Ramírez, C., Ferrando, R., Montecino, D., Lienlaf, M., 2019. Geología de las áreas Salar Punta Negra y Cerro Sur Bayo, región de Antofagasta, vols. 202–203. Servicio Nacional de Geología y Minería, Carta Geológica de Chile, Serie Geología Básica, Santiago, p. 130, 1 mapa escala 1:100.000.

Viramonte, J.G., Petrinovic, I.A., 1985. Cryptic and Partially Buried Calderas Aling a Strike-Slip Fault System in the Central Andes, pp. 317–320.

Warren, I., Archibald, D.A., Simmons, S.F., 2008. Geochronology of epithermal au-ag mineralization, magmatic-hydrothermal alteration, and supergene weathering in the El Penon district, northern Chile. Econ. Geol. 103 (4), 851–864. https://doi.org/10.2113/gsecongeo.103.4.851.

Yamaji, A., 2000. The multiple inverse method: a new technique to separate stresses from heterogeneous fault-slip data. J. Struct. Geol. 22, 441–452. https://doi.org/10.1016/S0191-8141(99)00163-7.

Yamaji, A., Otsubo, M., Sato, K., 2006. Paleostress Analysis Using the Hough Transform for Separating Stresses from Heterogeneous Fault-Slip Data, vol. 28, pp. 980–990. https://doi.org/10.1016/j.jsg.2006.03.016.

Yáñez, G., Rivera, O., 2019. Crustal dense blocks in the fore-arc and arc region of Chilean ranges and their role in the magma ascent and composition: breaking paradigms in the Andean metallogeny. J. South Am. Earth Sci. 93, 51–66. https://doi.org/10.1016/j.jsames.2019.04.006.

Zappettini, E. O. y G. Blasco, 2001. Hoja Geológica2569-II, Socompa. Provincia de Salta, vol. 260. Instituto de Geología y Recursos Minerales, Servicio Geológico Minero Argentino, Boletín, Buenos Aires, p. 62.

Zappettini, E.O., Miranda-Angles, V., Rodríguez, C., Palacios, O., Cocking, R., Godeas, M., Uribe-Zeballos, H., Vivallo, W., Paz, M.M., Seggiaro, R., Heuschmidt, B., Gardeweg, M., Boulangger Rondoy, E., Korzeniewski, L., Mpodozis, C., Carpio, M., y Rubiolo, D., 2001. Mapa metalogénico de la región fronteriza entre Argentina, Bolivia, Chile y Perú (14° S y 28° S). Publicación Geológica Multinacional 2, Santiago de Chile, p. 222.